T.R.
BOLU ABANT İZZET BAYSAL UNIVERSITY
INSTITUTE OF GRADUATE STUDIES
Department of Physics

PHOTOPHYSICAL PROPERTIES OF SOME NEW FLUORESCENT 1,2,4-OXADIAZOLES

MASTER OF SCIENCE

FARAH IMAD ABDULKAREEM AL-HAYALI

ACADEMIC SUPERVISOR
Assoc. Prof. Dr. MURAT OLUTAŞ
ACADEMIC CO-SUPERVISOR
Assoc. Prof. Dr. AKIN SAĞIRLI

BOLU, JANUARY - 2023

APPROVAL OF THE THESIS

PHOTOPHYSICAL PROPERTIES OF SOME NEW FLUORESCENT 1,2,4-OXADIAZOLES submitted by **Farah Imad Adulkareem AL-HAYALI** and defended before the Examining Committee Members listed below in partial fulfillment of the requirements for the degree of **Master of Science** in **Department of Physics, Institute of Graduate Studies of Bolu Abant Izzet Baysal University in 05.01.2023** by

Examining Committee Members	**Signature**
Supervisor Assoc. Prof. Dr. Murat OLUTAŞ Bolu Abant İzzet Baysal University	.....
Member Prof. Dr. Muhammet YILDIRIM Bolu Abant İzzet Baysal University	.....
Member Assoc. Prof. Dr. Atılgan ALTINKÖK National Defense University	.....

Prof. Dr. İbrahim KÜRTÜL

Director of Institute of Graduate Studies

ETHICAL DECLARATION

In this thesis dissertation that was properly prepared according to the Thesis Writing Rules of Bolu Abant İzzet Baysal University of the Institute of Graduates Studies, I hereby declare that;

- All data, information, and documents presented in the thesis were obtained in accordance with the academic and ethical rules,
- All data, documents, assessments, and results were presented in accordance with the scientific ethical, and moral rules,
- All works that were benefitted in the thesis were appropriately cited,
- No alteration was made in the data used,
- Study presented in this thesis is original,

Otherwise, I declare that I accept the loss of all my rights in case of any contradiction that may arise against me.

Based on the plagiarism report that was generated on the date of 11/12/2022 by using predetermined filtrations set by Directorate of Institute of Graduate Studies of the Turnitin program, a plagiarism detection software, the similarity index detected was 22 %.

_____

Farah Imad Adulkareem AL-HAYALI

ABSTRACT

PHOTOPHYSICAL PROPERTIES OF SOME NEW FLUORESCENT 1,2,4-OXADIAZOLES
MSC THESIS
FARAH IMAD ABDULKAREEM AL-HAYALI
BOLU ABANT IZZET BAYSAL UNIVERSITY
INSTITUTE OF GRADUATE STUDIES
DEPARTMENT OF PHYSICS
(SUPERVISOR: ASSOC. PROF. DR. MURAT OLUTAŞ)
(CO-SUPERVISOR: ASSOC. PROF. DR. AKIN SAĞIRLI)

BOLU, JANUARY 2023
(xv + 71)

In this thesis, we synthesized some new 1,2,4-oxadiazoles having aryl and styryl moieties functionalized with different electron-donating and -withdrawing groups, such as OCH_3, SCH_3, CN, and NO_2. The photophysical properties of the compounds were also investigated by utilizing UV-Vis absorption, steady-state fluorescence, and time-resolved fluorescence spectroscopy techniques, in detail. It was found that just the compounds with the structure comprising an electron-donating group on the aryl-moiety and an electron-withdrawing group on the styryl-moiety exhibit fluorescence emission in the solution. The absorption and fluorescence measurements have revealed that the spectral position of the fluorescence emission exhibits strong redshifted behavior with the increase in solvent polarity, while the absorption curve remains almost unchanged. In addition, the fluorescence quantum yield of both compounds was found to be in a decreasing trend with increasing solvent polarity, which suggests the dipole-dipole interactions between the fluorophore molecule having strong intramolecular charge transfer (ICT) characteristics and solvent. The quantum chemical calculations comprising density functional theory also elucidated the suggested strong ICT characteristic for both compounds. Furthermore, it was observed solid-state fluorescence emission in all compounds. The compounds with the structure comprising an electron-donating group on the aryl-moiety and an electron-withdrawing group on the styryl-moiety were found to exhibit relatively higher quantum yields among them. Also, it was found that the fluorescence quantum yield tends to decrease or increase depending on the type of substituent on the aryl and styryl moieties, and the results are well consistent with time-resolved fluorescence measurements. The findings revealed that the non-radiative decay rate in the emission mechanism of the compounds dominantly governs their fluorescence emission in solid-state, depending on the type of substituent on the aryl and styryl moieties.

KEYWORDS: 1,2,4-oxadiazoles, photophysical properties, fluorescence emission, solid-state emission, fluorescence quantum yield, fluorescence lifetime, substituent effect, and solvatochromism

ÖZET

BAZI YENİ FLORESAN 1,2,4-OKSADİAZOLLERİN FOTOFİZİKSEL ÖZELLİKLERİ
YÜKSEK LİSANS TEZİ
FARAH IMAD ABDULKAREEM AL-HAYALI
BOLU ABANT İZZET BAYSAL ÜNİVERSİTESİ
LİSANSÜSTÜ EĞİTİM ENSTİTÜSÜ
FİZİK ANABİLİM DALI
(TEZ DANIŞMANI: DOÇ. DR. MURAT OLUTAŞ)
(İKİNCİ DANIŞMAN: DOÇ. DR. AKIN SAĞIRLI)

BOLU, OCAK 2023
(xv + 71)

Bu tezde, farklı elektron-salıcı (OCH_3, SCH_3,) ve elektron-çekici (CN, NO_2) gruplarla foksiyonelleştirilmiş aril ve stiril parçalara sahip bazı yeni 1,2,4-oksadiazoller sentezlenmiştir. Buna ek olarak, bileşiklerin fotofiziksel özellikleri de UV-Vis soğurma, sabit-durum ve zamana çözünürlüklü floresan spektroskopileri kullanılarak ayrıntılı olarak araştırılmıştır. Sentezlenen bileşiklerin fotofiziksel özellikleri UV-Vis soğurma, sabit-durum floresan ve zamana bağlı floresan spektroskopi teknikleri kullanılarak ayrıntılı olarak çalışılmıştır. Elde edilen sonuçlar sentezlenen bileşikler arasında aril parçası üzerinde elektro-veren ve stiril parçası üzerinde ise elektron-çeken grup takılı bileşiklerin çözücü içinde floresan ışıması sergilediğini göstermiştir. Ayrıca, floresan ışımasının spektral konumunun çözücü polaritesinin artması ile güçlü bir kırmızıya kayma davranışı sergilediği, buna karşın soğurma eğrisinin spektral konumunun ise ortamın polaritesinden hemen hemen bağımsız davranışa sahip olduğu gözlemlenmiştir. Bununla beraber, her iki bileşiğin de floresan kuantum verimliliklerinin artan çözücü polaritesi ile azalma eğiliminde olduğu bulunmuştur. Bu sonuç güçlü molekül içi yük transferi özelliğine sahip ışıyıcı molekülleri ile çözücü molekülleri arasındaki dipol-dipol etkileşimlerinin bir sonucu olarak ortaya çıkmaktadır. Çözücü içinde ışıma yapabilen iki bileşik için önerilen güçlü molekül içi yük transferi karakteristiği, yoğunluk fonksiyonel teorisini (DFT) içeren kuantum kimyasal hesaplamalar kullanılarak ayrıca aydınlatılmıştır. Bunun dışında, sentezlenen tüm bileşiklerde katı hal floresan ışıması da gözlenmiştir. Tüm bileşikler arasında aril parçası üzerinde elektro-veren ve stiril parçası üzerinde ise elektron-çeken grup takılı bileşiklerin göreli olarak daha yüksek kuantum verimliliğe sahip oldukları bulunmuştur. Elde edilen sonuçlar, aril ve stiril kısımları üzerindeki fonksiyonel grupların elektron verme veya çekme özelliklerine bağlı olarak, bileşiklerin emisyon mekanizmasındaki ışımasız bozunma hızının katı haldeki floresan ışımalarını baskın şekilde yönettiğini ortaya çıkarmaktadır.

ANAHTAR KELİMELER: 1,2,4-oksadiazoller, fotofiziksel özellikler, floresan emisyonu, katı hal emisyonu, floresans kuantum verimi, floresans ömrü, sübstitüent etkisi ve solvatokromizm

TABLE OF CONTENTS

LIST OF FIGURES

Page

LIST OF TABLES

Page

LIST OF SCHEMES

Page

LIST OF ABBREVIATIONS AND SYMBOLS

LED : Light-emitting diodes

ICT : Intramolecular charge transfer

NMR : Nuclear magnetic resonance

CDI : 1,1'-Carbonyldiimidazole

DCC : Dicyclohexylcarbodimide

DCE : 1-[3-(Dimethylamino)propyl]-3-Ethylcarbodiimide

IR : Infrared

NH_2OH : Hydroxylamine

NH_3 : Ammonia

$ZnCl_2$: Zinc chloride

HCl : Hydrochloric

D : Donor

A : Acceptor

HOMO : Highest occupied molecular orbital

LUMO : Lowest unoccupied molecular orbital

TLC : Thin layer chromatography

UV : Ultraviolet

$KMnO_4$: Potassium permanganate

KBr : Potassium bromide

NaCl : Sodium chloride

$CDCl_3$: Deuterated chloroform

DMSO-d6 : Dimethyl sulfoxide-d6

CH_2Cl_2 : Dichloromethane

CH_3CN : Acetonitrile

Na_2SO_4 : Sodium sulfate

K_2CO_3 : Potassium carbonate

RXN : Reaction

TRF : Time-resolved fluorescence

ICCD : Intensified charge-coupled device

TCSPC : Time-correlated single photon counting

PL : Photoluminescence

PL QY : Fluorescence (or photoluminescence) quantum yield
ED : Electron-donating
EW : Electron-withdrawing
UV-Vis : Ultraviolet-visible
DFT : Density functional theory
MO : Molecular orbitals
TD-DFT : Time dependent-density functional theory
S_0 : Ground-state
S_1 : First excited state
S_2 : Second excited state
E_{ex} : Excitation energy
λ_{abs} : Absorption wavelength
f : Oscillator strength
μ_e : Dipole moment in the excited state
μ_g : Dipole moment in the ground state
λ_{PL} : Maximum emission wavelength

ACKNOWLEDGEMENTS

I would like to sincerely express thanks to my supervisor Assoc. Prof. Dr. Murat OLUTAŞ for his guidance, advice, criticism, encouragement, and insight throughout the research.

The author would like to thank my co-supervisor Assoc. Prof. Dr. Akın SAĞIRLI for his guidance and support with the synthesis and the structural characterizations of the organic compounds used in this study.

The author would also like to thank Havva ACAR for her help and endless support with the synthesis and IR Spectroscopy measurements of the organic compounds used in this study.

Finally, my greatest debt, as always, is to my family for their support, encouragement, and endless love they always give me.

This study was supported by the Research and Development Foundation of Abant İzzet Baysal University (BAP), Grant No: 2021.03.03.1515

1. INTRODUCTION

Fluorescent materials are commonly used in many areas such as fluorescent lamps, light-emitting diodes (LED), bio-labeling, and biosensors. Therefore, the interest and research to improve the properties of the known materials or find new materials have increased in the last twenty years. Fluorescent organic compounds are among the optical material groups, which have been studied extensively in the literature, due to their photophysical properties and advantages such as easy synthesis, low cost, and low toxicity compared to their inorganic conjugates. The photophysical properties of these compounds depend on the relevant electronic transitions. Hence, if the structure-property relationship is known for a particular class of molecule, the optical properties of organic materials can be fine-tuned by structural design strategies.

Under photoexcitation, the emission kinetics of conventional organic molecules, such as rhodamine, fluorescein, and BODIPY, are governed by delocalized optical transitions over the entire structure. The photophysical properties of such organic molecules can be roughly characterized by absorption and emission curves with mirror symmetry relative to each other, and a small Stokes shift that is independent of the polarity of the solvent. On the other hand, in organic compounds consisting of electron-donating (donor) and -withdrawing (acceptor) groups, the emission is generally caused by intramolecular charge transfer transitions (ICT) (1–3). These materials have broad absorption and emission curves in polar environments compared to conventional organic compounds, besides, they can exhibit large Stokes shifts depending on the polarity of the surrounding solvent environment. In other words, the structural modification of electron-donating and -withdrawing groups on the main skeleton allows charge separation in these compounds, which enables the tunning of photophysical properties such as spectral position, fluorescence quantum yield, and fluorescence lifetime. This property makes these materials valuable for applications such as organic photovoltaics (4), organic light-emitting diodes (5,6), polarity or viscosity-sensitive sensors (7,8), and chemo-sensors (9).

Oxadiazole-based compounds are one of the most studied D-π-A organic systems in the literature, and their photophysical properties can be tuned with

electron-donating and -withdrawing groups attached to them. 1,3,4-oxadiazoles, one of the heterocyclic compounds formed by different combinations of two nitrogen, one oxygen, and two carbon atoms, increase the fluorescence properties of the group to which they are attached due to their excellent electron transport functionality. Furthermore, their properties, such as wide band gap and thermal stability, make oxadiazole derivatives a promising material for organic-based optoelectronic applications with high electron mobility (10). On the other hand, 1,2,4-oxadiazole, another member of the oxadiazole family, has made a name for itself in the literature with their pharmacological properties until now (11). However, there are limited studies on the photophysical properties of this isomer of the oxadiazole family, in the literature (12–16). This makes 1,2,4-oxadiazole derivatives, which can show fluorescence properties, among the interesting materials of the literature in favor of understanding the photophysical properties and emission mechanisms, in addition to their important pharmacological effects.

The following sections will summarize the theoretical background of the synthesis of the 1,2,4-oxadiazoles and their photophysical properties published in the literature.

1.1 Oxadiazoles

Five-membered oxygen-nitrogen-containing heterocycles, namely, oxadiazoles, have vital importance for synthetic chemists due to not only their diverse biological activity but also being a part of many natural products. There are different isomeric forms such as 1,2,3-, 1,2,4-, 1,2,5- and 1,3,4-oxadiazoles depending on the position of nitrogen and oxygen on the ring (17–19) (see Figure 1.1).

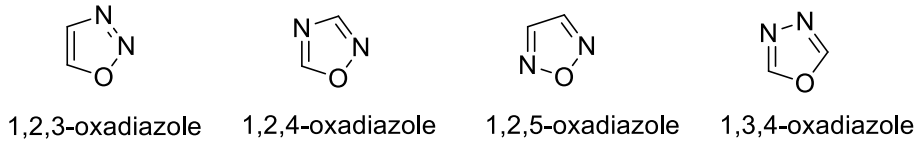

Figure 1.1. Different isomeric forms of oxadiazoles.

From a pharmacological aspect of view, several oxadiazole-containing heterocycles are in a late-stage clinical trial. For example, Zibotentan and Albatrate are both promising molecules having the potential for drug candidates exhibiting as anticancer agents and treatment of cystic fibrosis, respectively (20,21). So far, a new compound bearing oxadiazole moiety, Raltegravir, an antiretroviral drug for the treatment of HIV infection, has been launched on the Marketplace (22) (see Figure 1.2). Moreover, several oxadiazoles exist in literature exhibiting a wide range of biological activities such as anti-fungal (23), anti-inflammatory (24), anti-cancer (25), and anti-infection (26).

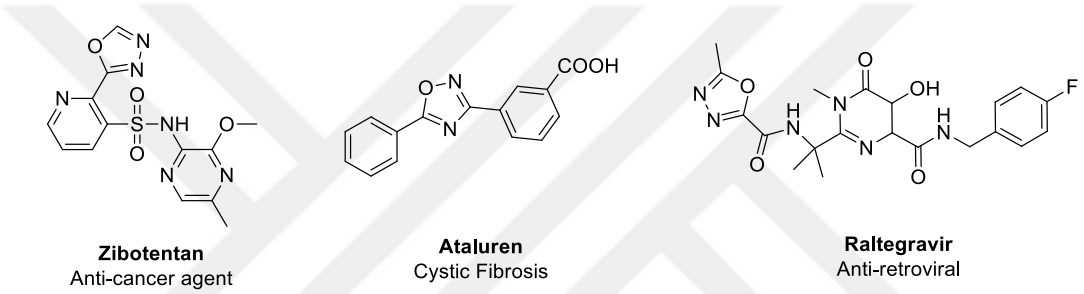

Figure 1.2. Some important drug candidates having oxadiazole moiety.

On the other hand, apart from their pharmacological activities, the focus is recently placed on their photophysical property. 1,3,4- oxadiazoles and 1,2,4-oxadiazoles are known as the most commonly studied regioisomers that have been incorporated in many functional fluorescent molecules (27). Due to their good luminescence and high thermal stability, aryl-1,3,4-oxadiazoles and their vinylogous counterparts have been widely used for the synthesis of fluorescent heterocycles (28). However, there are limited studies involving the synthesis and photophysical properties of new 1,2,4-oxadiazoles (see Figure 1.3) (29).

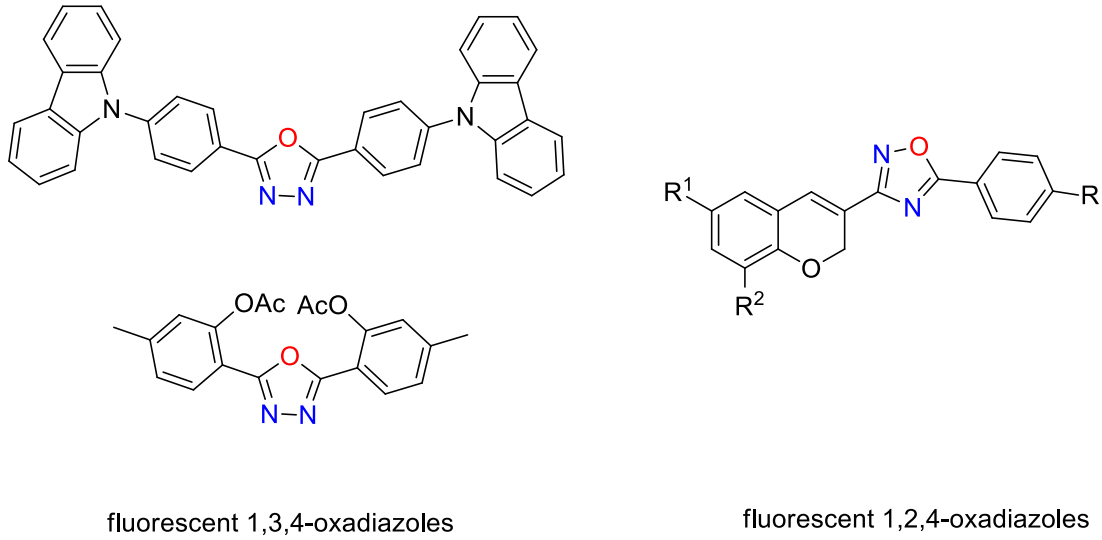

Figure 1.3. Some fluorescent 1,3,4- and 1,2,4-oxadiazole-containing compounds.

1.2 1,2,4-Oxadiazoles

Surfactants 1,2,4-oxadiazoles are of significant importance among the five-membered heterocycles bearing only N-O atoms. They have many applications, especially, in the field of pharmacology exhibiting remarkable biological activity such as anti-cancer (25), anti-inflammatory (30), anti-oxidant (31), anti-viral, and inhibitors of protein tyrosine phosphatases (32). Also, some commercially available drugs, pleconaril (anti-infective) (33), prenoxdiazine (cough suppressant) (34), and oxolamine (anti-inflammatory) (35) contain 1,2,4-oxadiazole core in their skeleton (see Figure 1.4).

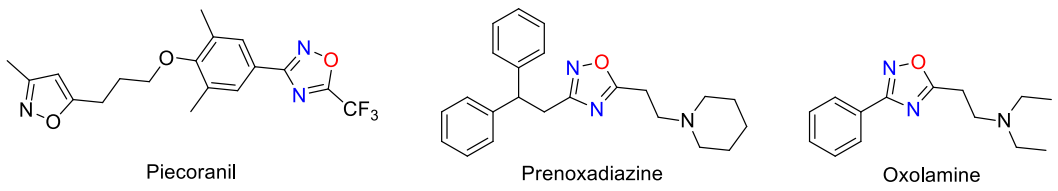

Figure 1.4. Some commercially available 1,2,4-oxadiazole containing drugs.

1.2.1 Chemistry of 1,2,4-Oxadiazoles

The 1,2,4-oxadiazole bears 2 nitrogen and one O in its ring. The ring is planar and has an aromatic character considering the bond lengths of the N2-C3 and N4-C5 bonds. In addition, this aromatic behavior is supported by X-ray diffraction analysis, NMR spectra, IR spectra, and mass measurements (36). Whereas disubstituted 1,2,4-oxadiazoles can be regarded as thermally quite stable, mono and unsubstituted ones are considerably less stable. 1,2,4-Oxadiazoles show an extremely low reactivity towards electrophilic attack at carbon, the only known example being electrophilic mercuriation of the 5-unsubstituted systems. Disubstituted 1,2,4-oxadiazoles can withstand boiling aqueous sodium hydroxide or hydrochloric acid, whereas monosubstituted systems readily undergo hydrolysis under such conditions (37).

1.2.2 Synthesis of 1,2,4-Oxadiazoles

1.2.2.1 1,3-Dipolar Cycloaddition Reactions of Nitrile Oxides with Nitriles

One of the most common methods for the formation of 1,2,4-oxadiazole derivatives is 1,3-dipolar cycloaddition of nitrile oxide with nitriles. As a 1,3-dipole, nitrile oxide **3**, can be obtained from nitroalkane **2** in the presence of phenyl isocyanate and dehydrohalogenation of imidoyl halides **1**. Aryl-substituted nitriles are commonly employed as dipolarophilic agents. However, the reactivity of aliphatic nitriles is relatively low that generally requires Lewis acid. In this route, in situ generated nitrile oxide is treated with corresponding nitrile derivatives to give desired 1,2,4-oxadiazole compounds **4** (see Scheme 1.1) (38,39).

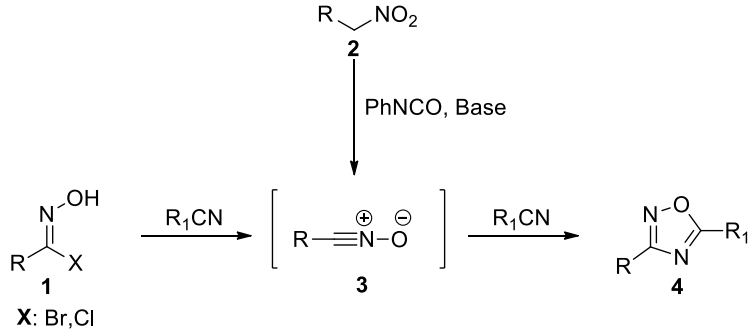

Scheme 1.1. Synthesis of 1,2,4-oxadiazoles **4** via 1,3-dipolar cycloaddition of nitrile oxides **3** with nitriles.

1.2.2.2 1,3-Dipolar Cycloaddition Reactions of Nitrile Oxides with Imines

In situ generated nitrile oxide **3** with the C=N (imine) **5** bond to provide dihydro-1,2,4-oxadiazole **6** which then undergoes aromatization or oxidation with the loss of XY (see Table 1.1) to yield 1,2,4-oxadiazoles **4**. The wide diverse range functionalities of C=N bond allow the 1,3-dipolar cycloaddition reaction in such a manner involving guanidine, 1-azetidine, imidates, amidines, and certain 2-pyrazolines (40–42).

Table 1.1. Synthesis of 1,2,4-oxadiazoles via 1,3-dipolar cycloaddition of nitrile oxides with imine derivatives.

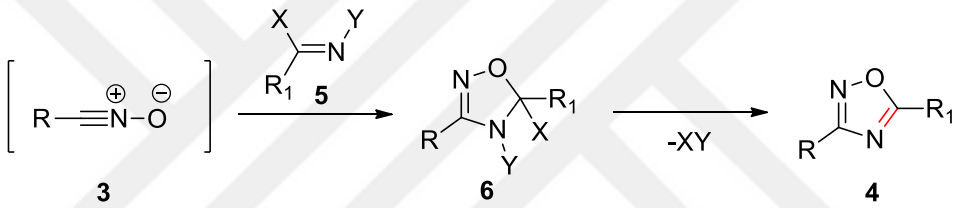

R	R_1	Yield %
4-OH-3,5,-$(tBu)_2C_6H_2$	NH_2	16
4-OH-3,5,-$(tBu)_2C_6H_2$	$NHC(=NH)NH_2$	49
Ph	CH_2CH_2NHMe	53
CO_2Et	CMe_2CMe_2F	87
Ph	CMe_2CMe_2F	81

1.2.2.3 Acylation of Amidoximes with Derivatives of Carboxylic Acids

The well-known route for the achievement of 1,2,4-oxadiazoles is the reaction of amidoximes with a variety of carboxylic acid derivatives such as acid chlorides **12**, esters, and anhydrides **11**. As a key reactant, amidoximes **9**, can be achieved by the reaction of nitrile **7** with NH_2OH or by the chlorination of oxime **8** followed by a reaction with ammonia. On the other hand, the corresponding reaction involves two sequential steps; O-acylation of amidoximes followed by cyclodehydration (see Scheme 1.2). It is noteworthy saying that the carboxylic acids

generally require CDI (1,1'-carbonyldiimidazole), DCC (dicyclohexylcarbodimide), and DCE (1-[3-(dimethylamino)propyl]-3-Ethylcarbodiimide) for the activation through the reaction (43).

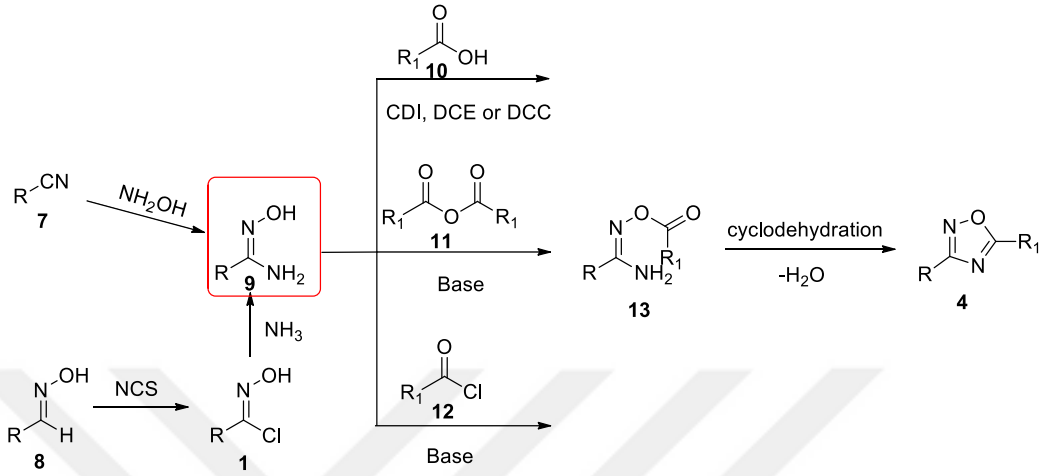

Scheme 1.2. Synthesis of 1,2,4-oxadiazole derivatives **4** via the reaction of amidoxime **9** with carboxylic acid derivatives.

Some 1,2,4-oxadiazoles **4** were prepared by using carboxylic acids **14** and benzamidoximes **9** in the presence of ethyl chloroformate **15** that accelerates the reaction by converting carboxylic acid **14** into more reactive acid anhydride (44).

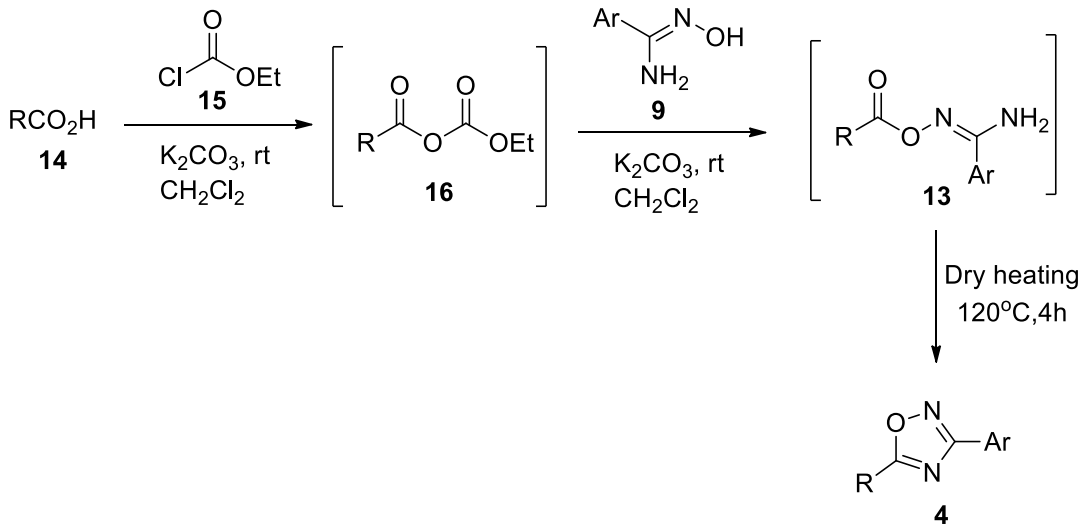

Scheme 1.3. Synthesis of 1,2,4-oxadiazoles by utilizing carboxylic acid **14** and arylamidoximes **9**.

A variety of coupling reagents and their effect on the conversion of the carboxylic acid into corresponding 1,2,4-oxadiazoles upon the treatment with amidoximes were studied by Liang and co-workers. The success of DCC on carboxylic acid conversion has been known for many years. The study exhibited that the derivatives of DCC like CDI, EDC, and BOP-Cl have proved to be successful under neutral conditions (see Table 1.2) (45,46).

Table 1.2. Synthesis of 1,2,4-oxadiazoles **4** from carboxylic acids **14** and amidoximes **9** by using coupling reagents.

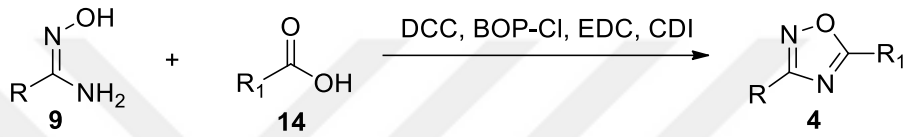

R	R_1	Coupling Reagent	Solvent	Yield %
4-$MeOC_6H_4$	4-NCC_6H_4	CDI	DMF	60
4-Tol	4-$MeOC_6H_4$	EDC	Diglyme	50-60
4-Tol	4-$NO_2C_6H_4$	EDC	Diglyme	50-60
4-Tol	Bu	EDC	Diglyme	60
4-Tol	Bu	DCC	Diglyme	54
4-Tol	Bu	BOP-Cl	Diglyme	64
4-Tol	Pr	EDC	Diglyme	63

1.2.2.4 Other Methods for Preparation of 1,2,4-Oxadiazoles

A range of alkyl, aryl, and heteroaryl substituted nitriles **7** undergo reaction with some amidoximes **9** to provide initially the 2,3-dihydrooxadiazol-3-amine, then by the extrusion of NH_3 to give 1,2,4-oxadiazoles **4**. The reaction seems to be effective in the presence of $ZnCl_2$ and HCl (47).

Table 1.3. 1,2,4-Oxadiazoles from Nitriles and Amidoximes.

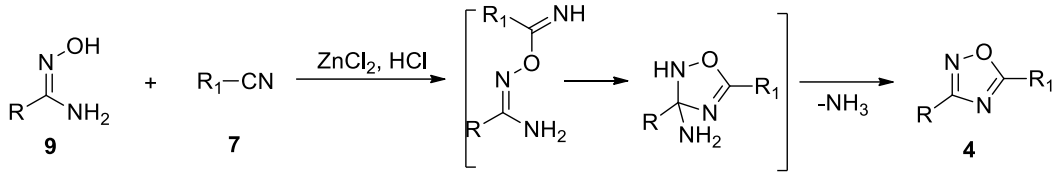

R	R_1	Yield %
5-nitro-2-furyl	Me	88
5-nitro-2-furyl	CH_2Cl	67
5-nitro-2-furyl	Bn	63
CH_2Cl	5-nitro-2-furyl	66
CH_2Cl	CH_2Cl	64
3-$NO_2C_6H_4$	CH_2CH_2Cl	42
Ph	CH_2CH_2Cl	40
Ph	CH_2CO_2Et	47
Ph	Ph	70

Another method is suggested by Yarovenko and co-workers. The utilizing triethylorthoformate **17** bearing alkyl and aryl groups with amidoxime derivatives **9** gives access to a variety of 1,2,4-oxadiazoles **4** in good to excellent yield (48).

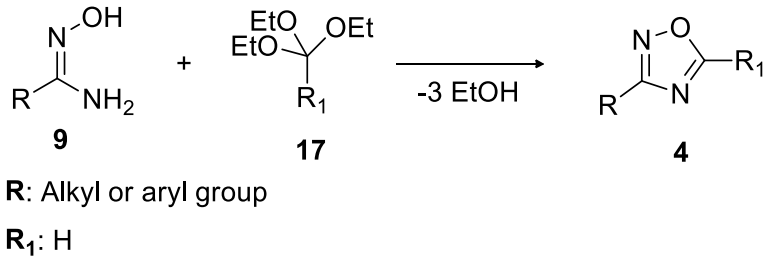

Scheme 1.4. Synthesis of 1,2,4-oxadiazole via the reaction of amidoxime **9** with triethylorthoformate **17**.

1.3 Literature Review on Photophysical Properties of 1,2,4-Oxadiazoles

Nowadays, organic molecules with delocalized π-electron systems are among the interesting materials for optoelectronic applications using advanced functional materials. Their easy synthesis, well-known and modifiable molecular structures, and predictable, typical, and unique properties make these hetero-aromatic π-conjugated systems stand out against many materials. In addition, these organic π-conjugated systems, which can be functionalized with electron-donating and -withdrawing groups, are commonly called push-pull systems in the literature and are a part of organic π-systems. Intramolecular charge transfer (ICT), which occurs with the interaction between electron-donating (donor, D) and -withdrawing (acceptor, A) groups in such D-π-A systems, changes the optical properties of these materials and is also responsible for the polarization of the molecular system and the molecular dipole formation in that structure (49). 1,3,4-oxadiazole is one of the π-conjugated systems that is frequently used as a π-bridge in the literature to provide electron flow between donor and acceptor groups in D-π-A systems, where the ICT mechanism plays an active role (50,51). Besides its excellent electron-donating and electron-transport capabilities make 1,3,4-oxadiazol a popular n-type material, these properties allow it to be used as a fluorescent material in applications such as chemo-sensors (51,52), organic semiconductors (53–55), and electroluminescent devices (56,57).

Another isomer of the oxadiazole family is 1,2,4-oxadiazole. Compared with 1,3,4-oxadiazole derivatives, 1,2,4-oxadiazole derivatives shine out in the literature with their biological and pharmacological properties to date (58–60). However, although there are many studies on its biological and pharmacological activities and properties in the literature, there are very few studies reported on 1,2,4-oxadiazole derivatives with fluorescent properties. S. Buscemi et al., in 2006, reported that the star-shaped large molecules obtained by adding fluorinated 1,2,4-oxadiazole ring on the triethanolamine body displayed fluorescence emission covering the purple and blue regions of the electromagnetic spectrum (between 360 and 500 nm) in acetonitrile (12). In another study conducted in the same year, the photophysical properties of similar molecules, obtained by positioning alkoxy and

benzyl groups on 1,2,4-oxadiazole and 1,3,4-oxadiazole skeletons, were comparatively investigated. In this study, which was carried out using the alkoxy groups with different carbon lengths, all derivatives with 1,3,4-oxadiazoles displayed strong fluorescence emission in chloroform, while just the compound comprising 12 carbon chains among the 1,2,4-oxadiazoles, all in the liquid crystal structure, exhibited a fluorescence emission at 350 nm with 15% quantum yield (13). In addition, L.S. Liao et al., used 1,2,4-oxadiazole as an electron-withdrawing unit for the first time in the molecule they synthesized in 2014, and they stated that these bipolar molecules emit blue fluorescence emission (440-450 nm) in dichloromethane (see Figure 1.5a) (14). In that year, the same group showed that the bipolar 1,2,4-oxadiazole derivative exhibited both fluorescence and phosphorescence emissions by binding the electron-donating carbazole group to the 1,2,4-oxadiazole ring (Figure 1.5b) (15). K. Singh et al., in a study they conducted in 2017, obtained a new hybrid structure that exhibited a fluorescence emission in the blue side of the visible region (446-468 nm) by binding the coumarin molecule to the 5-position on the 1,2,4-oxadiazole ring (Figure 1.5c) (16).

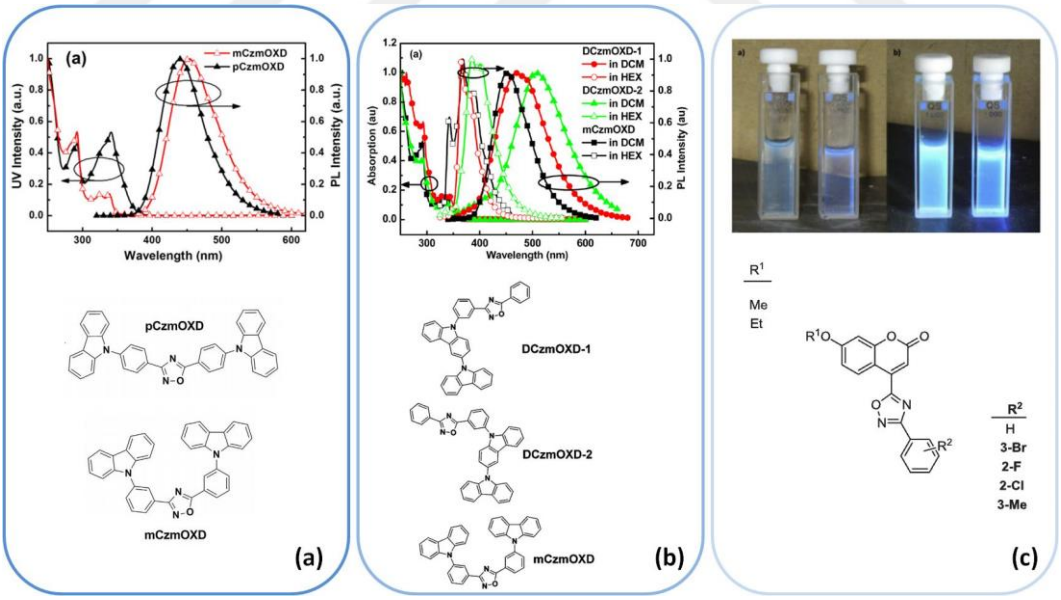

Figure 1.5. The exemplary cases reported by different groups in the literature for the 1,2,4-oxadiazole derivatives exhibiting fluorescence emission. The figures are adapted from the literature (14–16).

2. AIM AND SCOPE OF THE STUDY

As summarized in the previous section, although 1,2,4-oxadiazole has unique structural and electronic properties, so far, most of the studies included the photophysical properties of the compounds bearing oxadiazole ring and published in the literature, are based on 1,3,4-oxadiazoles. There are limited studies that have reported fluorescence emission of the small molecules (micro-molecules) of 1,2,4-oxadiazole in a solvent medium. Moreover, even though a few published works are reporting solid-state fluorescent emission for the polymer-like macro-molecules bearing 1,2,4-oxadiazole, to the best of our knowledge, no reported study on micro-molecules of the 1,2,4-oxadiazole that exhibited fluorescence emission in solid-state up to now. However, the structural asymmetry of the 1,2,4-oxadiazoles (i.e., meta-linked configuration) enables new molecule designs, and possible modifications on alpha- and beta-carbon positions can cause changes in the HOMO-LUMO energy levels of the target molecule. In conclusion, the great potential in the development of new materials with the ability to emit fluorescence and/or phosphorescence emission derived from 1,2,4-oxadiazole heterocycle that can be used in biological and optoelectronic applications has not been fully exploited yet. In this context, the aims and objectives of our master thesis can be summarized as follows.

In this study, we first aim to synthesize some new luminescent molecules with a meta-linkable 1,2,4-oxadiazole heterocycle in the main body. Depending on whether the electron-donating and electron-withdrawing groups substituted 3 and 5 positions of the oxadiazole ring and their electron-donating and withdrawing abilities, the photophysical properties of the compounds in the solution are going to be investigated. In addition, it is also aimed to investigate how the photophysical properties of the compounds can be affected by the polarity of the solvent. Furthermore, we purpose to show the solid-state photoluminescence emission properties in the small molecules of the 1,2,4-oxadiazoles for the first time in the literature.

3. MATERIALS AND METHODS

3.1 Chemicals and Instruments

All the reagents and solvents were purchased from commercial sources and utilized without any additional purification. Standard techniques were used to dry the solvents. Thin layer chromatography (TLC) was used to keep track of the reactions. The chromatograms were seen using UV light and $KMnO_4$. IR spectra were recorded on a Shimadzu FT-IR-8400S instrument (KBr pellet or NaCl discs) and a Shimadzu FT-IR Spectrometer with an ATR system. ^{1}H- and ^{13}C- NMR spectra were recorded on VARIAN spectrometers (400 MHz for proton and 100 MHz for carbon) spectrometer at ambient temperature. All NMR spectra were obtained in $CDCl_3$ or DMSO-d6 using Me_4Si as an internal standard at 400 MHz for proton and 100 MHz for carbon-13, respectively. The following acronyms are used to describe peak multiplicities: s stands for singlet; d stands for doublet; q stands for a quartet. On Merck silica gel F254 plates, analytical TLC was performed. Ethyl acetate/n-hexane were employed as eluents in flash chromatographic purifications using Merck Silica gel 60 (230–400 mesh ASTM) as the stationary phase. Melting points (mp) were determined using a MELTEMP instrument in open capillary tubes and are uncorrected.

3.2 Synthesis of Precursors and Styryl-1,2,4-Oxadiazoles

3.2.1 General Procedures for Preparation of Cinnamic Acids **20** (61,62)

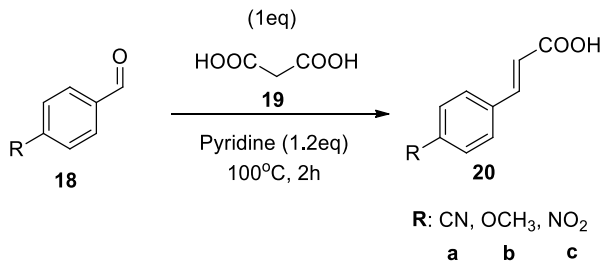

To a mixture of corresponding aldehyde **18** (10 mmol) and malonic acid **19** (1.04 g, 10 mmol) in a round-bottomed flask, pyridine (0.96 mL, 12 mmol) was added, and the reaction mixture was heated to 100°C for 2-3 hours. After completion, the reaction mixture was cooled and diluted with 40 mL of water. The formed acid was dissolved by the addition of concentrated aqueous NH_3, the solution was filtered and washed with water (2x10 mL). The combined filtrates

were acidified with an excess of dilute (1:1) HCl, then cooled and allowed to stand in an ice bath for 1 h. It was filtered, washed with water, and dried to afford the corresponding cinnamic acids **20 a-c** in good yields.

3.2.2 General Procedures for Preparation of Cinnamic Acid Chlorides **21** (61,62)

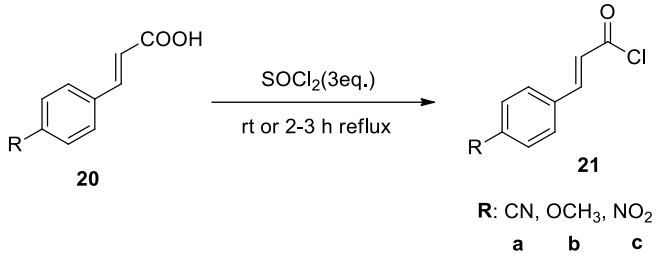

Corresponding cinnamic acid **20** (3 mmol) was mixed with thionyl chloride (0.4 mL, 0.65 g, 9 mmol) under the N_2 atmosphere. The resulting mixture was either stirred in CH_2Cl_2 at room temperature or refluxed in CH_3CN for 3-4 hours. The reaction mixture was cooled and evaporated to afford corresponding cinnamic acid chlorides **21 a-c** as powder or crystals.

(*E*)-4-nitrocinnamoyl chloride 21c

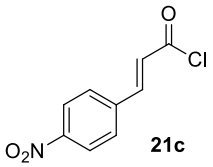

Treating oxalyl chloride (1.72 mL, 2.54 g, 20.0 mmol) with a mixture of (*E*)-p-nitrocinnamic acid (1.93 g, 10 mmol) and *N*,*N*-dimethylformamide (5-6 drops) in dry CH_2Cl_2 (40 mL) at 0^oC under N_2 atmosphere for 2.5 hours to give **21c** (2.00 g), yield: quantitative. bright yellow crystals. m.p. 293-294˚C. Rf: 0.90 (50% ethyl acetate/hexane). IR (KBr): νmax/cm^{-1} = 3107 (-C=CH), 3061 (arom. C-H), 2922, 1753 (C=O), 1626 (C=C), 1518, 1344, 1265, 1101, 1026, 977, 840, 748, 665 cm^{-1}; ^1H NMR (400 MHz, DMSO-d6) δ 8.21 (d, 2H, J = 8.8 Hz), 7.95 (d, 2H, J = 9.2 Hz), 7.67 (d, 1H, J = 16.0 Hz), 6.73 (d, 1H, J = 16.0 Hz); ^{13}C NMR (100 MHz, DMSO-d6) δ 124.3, 124.6, 129.9, 141.4, 142.0, 148.6, 167.7

3.2.3 General Procedure for the Preparation of Amidoxime Derivatives (63)

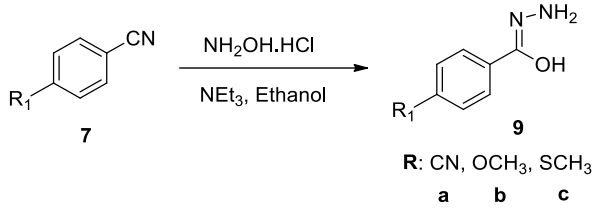

To a solution of benzonitrile derivatives **7** (37.0 mmol) and triethylamine, Et_3N (101 g, 56.7 mmol) in 100 mL ethanol, $NH_2OH.HCl$ (4.05 g, 56.7 mmol) was added slowly by stirring until all $NH_2OH.HCl$ was dissolved. The mixture was stirred under reflux for 24 h. Solvent was evaporated under the reduced pressure and the crude product was extracted with ethyl acetate: water (25mL:25mL)x4. Combined organics were washed with brine solution and dried with anhydrous Na_2SO_4. The solvent was evaporated under reduced pressure and the product **9 a-c** was crystallized from benzene.

3.2.4 General Procedure for the Preparation of Styryl-1,2,4-Oxadiazole Derivatives (64,65)

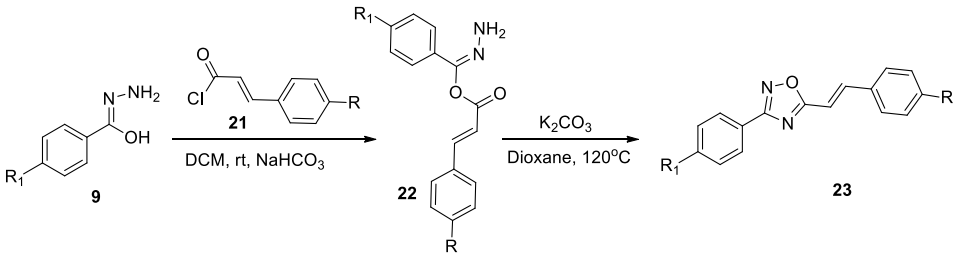

Cinnamic acid chloride (11 mmol) in CH_2Cl_2 was added dropwise into benzamidoxime derivatives (10 mmol) dissolved in CH_2Cl_2 (100ml). The mixture was allowed to stir at room temperature for 1-3 hours. The reaction was then washed with saturated $NaHCO_3$ solution (100 ml). The resulting organic fraction was washed with 2X50 ml water. The organic portion was dried over Na_2SO_4 and

filtered. The mixture was concentrated under a vacuum to give crude compound **22** in high yield.

Intermediate product **22** (5 mmol) and K_2CO_3 (5 mmol, 690 mg) were allowed to stir in dioxane (100ml) at 120°C for 12 hours. The progress of the reaction was then monitored by thin-layer chromatography. After completion of the reaction, the solvent was removed in vacuo and the crude product was purified by column chromatography. Target 1,2,4 oxadiazoles **23 a-f** were obtained in medium-high yields.

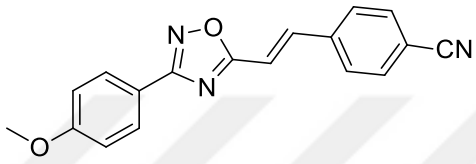

(*E*)-4-(2-(3-(4-methoxyphenyl)-1,2,4-oxadiazol-5-yl)vinyl)benzonitrile 23a (RXN-1) White solid (68%) IR (KBr, cm^{-1}): 2226 (CN), 1643, 1607 (C=N), 1537, 1414, 1363, 1245, 1170, 1027, 969, 836, 547. ^{1}H NMR (400 MHz, $CDCl_3$) δ 8.07 (d, J = 8.9 Hz, 2H), 7.87 (d, J = 16.4 Hz, 1H), 7.73 (q, J = 8.5 Hz, 4H), 7.16 (d, J = 16.4 Hz, 1H), 7.03 (d, J = 8.9 Hz, 2H), 3.90 (s, 3H). ^{13}C NMR (101 MHz, $CDCl_3$) δ 174.21, 168.78, 162.22, 140.14, 138.81, 132.98, 129.23, 128.39, 119.18, 118.48, 114.49, 113.89, 55.59.

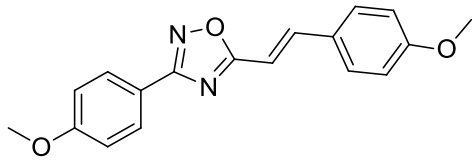

(*E*)-3-(4-methoxyphenyl)-5-(4-methoxystyryl)-1,2,4-oxadiazole 23b (RXN-2) Light yellow solid (60%) IR (KBr, cm−1): 1644, 1600 (C=N), 1536, 1415, 1362, 1244, 1170, 1029, 969, 839, 517. ^{1}H NMR (400 MHz, $CDCl_3$) δ 8.04 (d, J = 8.9 Hz, 2H), 7.80 (d, J = 16.4 Hz, 1H), 7.54 (d, J = 8.7 Hz, 2H), 6.98 (d, J = 8.9 Hz, 2H), 6.93 (d, J = 8.8 Hz, 2H), 6.90 (d, J = 16.3 Hz, 1H), 3.86 (s, 3H), 3.84 (s, 3H). ^{13}C NMR (101 MHz, $CDCl_3$) δ 175.29, 168.26, 161.81, 161.49, 142.10, 129.56, 128.98, 127.19, 119.47, 114.47, 114.19, 107.80, 55.40, 55.36.

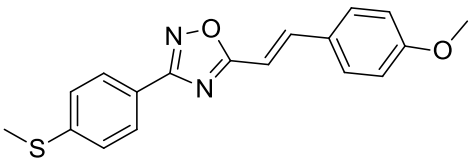

(*E*)-5-(4-methoxystyryl)-3-(4-(methylthio)phenyl)-1,2,4-oxadiazole 23c (RXN-3) Light yellow solid (58%) IR (KBr, cm^{-1}): 1638, 1598 (C=N), 1535, 1405, 1358, 1243, 1178, 1030, 966, 821, 566. ^{1}H NMR (400 MHz, $CDCl_3$) δ 8.04 (d, J = 8.6 Hz, 2H), 7.85 (d, J = 16.3 Hz, 1H), 7.58 (d, J = 8.7 Hz, 2H), 7.34 (d, J = 8.6 Hz, 2H), 6.96 (d, J = 9.3 Hz, 3H), 3.87 (s, 3H), 2.55 (s, 3H). ^{13}C NMR (101 MHz, $CDCl_3$) δ 175.52, 168.25, 161.59, 142.74, 142.37, 129.64, 127.69, 127.17, 125.85, 123.33, 114.53, 107.70, 55.46, 15.14.

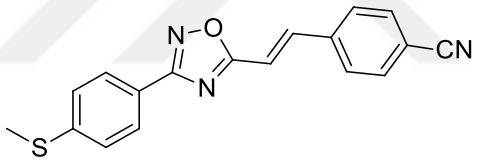

(*E*)-4-(2-(3-(4-(methylthio)phenyl)-1,2,4-oxadiazol-5-yl)vinyl)benzonitrile 23d (RXN-4) Light yellow solid (67%) IR (KBr, cm^{-1}): 2223 (CN), 1650, 1601 (C=N), 1531, 1407, 1363, 1245, 1183, 1091, 981, 817, 546. ^{1}H NMR (400 MHz, $CDCl_3$) δ 8.02 (d, J = 8.4 Hz, 2H), 7.86 (d, J = 16.4 Hz, 1H), 7.72 (q, J = 8.5 Hz, 4H), 7.34 (d, J = 8.4 Hz, 2H), 7.15 (d, J = 16.4 Hz, 1H), 2.54 (s, 3H). ^{13}C NMR (101 MHz, $CDCl_3$) δ 174.27, 168.60, 143.24, 140.20, 138.60, 132.87, 128.29, 127.73, 125.88, 122.89, 118.35, 113.65, 77.39, 77.08, 76.76, 15.11.

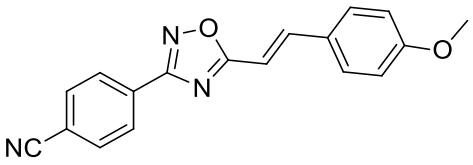

(***E***)**-4-(5-(4-methoxystyryl)-1,2,4-oxadiazol-3-yl)benzonitrile 23e (RXN-5)** Yellow solid (65%) IR (KBr, cm^{-1}): 2230 (CN), 1631, 1599 (C=N), 1538, 1413, 1355, 1250, 1173, 1018, 971, 821, 550. ^{1}H NMR (400 MHz, $CDCl_3$) δ 8.27 (d, J = 8.6 Hz, 2H), 7.88 (d, J = 16.3 Hz, 1H), 7.82 (d, J = 8.6 Hz, 2H), 7.60 (d, J = 8.7 Hz, 2H), 6.99 (d, J = 8.8 Hz, 2H), 6.94 (d, J = 16.3 Hz, 1H), 3.89 (s, 3H). ^{13}C NMR (101 MHz, $CDCl_3$) δ 176.50, 167.49, 162.01, 143.33, 132.84, 131.53, 129.98, 128.18, 127.13, 118.50, 114.79, 107.39, 55.68.

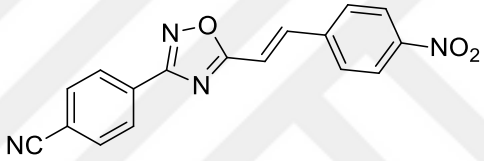

(*E*)-4-(5-(4-nitrostyryl)-1,2,4-oxadiazol-3-yl)benzonitrile 23f (RXN-6) Dark yellow solid (62 %) IR (KBr, cm^{-1}): 2162 (CN), 1637, 1597 (C=N), 1537, 1405, 1337, 1182, 1109, 1027, 971, 758, 688. ^{1}H NMR (400 MHz, $CDCl_3$) δ 8.30 (d, J = 8.8 Hz, 2H), 8.02 (d, J = 8.5 Hz, 2H), 7.91 (d, J = 16.4 Hz, 1H), 7.76 (d, J = 8.8 Hz, 2H), 7.33 (d, J = 8.5 Hz, 2H), 7.19 (d, J = 16.4 Hz, 1H), 2.54 (s, 3H). ^{13}C NMR (101 MHz, $CDCl_3$) δ 174.35, 168.86, 148.79, 143.49, 140.62, 139.88, 130.86, 128.73, 127.92, 126.07, 124.61, 123.66, 114.54, 15.31.

3.3 Optical Characterization of 1,2,4-Oxadiazole Derivatives

Steady-state linear absorption (i.e., UV-Vis absorption) and fluorescence emission spectroscopy are generally used in the literature as powerful and useful methods to investigate the photophysical properties of organic materials. In addition, time-resolved fluorescence (TRF) spectroscopy is commonly employed to understand the emission kinetics in fluorescent materials. Here, the techniques used for determining the photophysical properties of 1,2,4-oxadiazole derivatives are summarized with experimental details within the concept of the thesis.

3.3.1 UV-Vis Absorption Spectroscopy

Linear absorption measurement is generally performed to provide information about the optical properties of a material in the ground state that comes out of the interaction of light with the material. Briefly, in the absorption measurements, to excite the material with a light having a fixed wavelength, a full-spectrum light source with a monochromator is utilized. In addition, a photodetector is used to collect the transmitted light through the material in the solution. During the measurement, the cuvette filled with the material dissolved in a solvent is located between the monochromator and the photodetector, and the material is excited by scanning with the monochromatic light in a fixed wavelength interval. Then, the absorption of the material is determined by comparison of the intensity of the transmitted light through the sample cuvette to that of the reference cuvette filled just with the solvent.

The absorption measurements in the concept of this study were performed using the double-beam spectrophotometer (Hitachi U-2900) at room temperature, for the wavelength range of 200-800 nm. During the measurements, the concentration of the solutions was kept at 0.01 μM in toluene, and the quartz cuvettes with a 1cm optical path were used. All measurements were also repeated for chloroform and 1,2-dichloroethane. In addition, the molar absorptivity (or molar extinction coefficient) of the material dissolved in the solvent was determined according to the Lambert-Beer law (66)**,**

$$A = \varepsilon lC \tag{3.1}$$

where A is absorbance, ε is the molar absorptivity, l is the distance taken by the light in the cuvette (i.e., the width of the cuvette), and C is the concentration of the solution.

3.3.2 Steady-State Fluorescence Spectroscopy

Steady-state fluorescence spectroscopy is commonly utilized for characterizing the optical properties of fluorescent materials in the excited state. Briefly, in fluorescence spectroscopy, the target material is exposed to a beam of light having a fixed wavelength to excite it. To this end, a full-spectrum light source with a monochromator, or a laser is used as an excitation source with a fixed wavelength. In addition, using a monochromator positioned perpendicularly to the excitation beam, the emitted photons by the excited material are collected. During the measurement, the monochromator scans a broad wavelength range to collect the photons having different wavelengths.

In this study, fluorescence measurements of the 1,2,4-oxadiazole derivatives in solution were carried out by using Hitachi F-4500 Fluorescence Spectrophotometer. All measurements were taken in quartz cuvette at room temperature, and the concentration of the samples was kept at 0.01 μM in solution to eliminate the self-absorption effects. The measurements were performed for the solvent mediums having different polarities such as toluene, chloroform, and 1,2-dichloroethane.

On the other hand, the solid-state photoluminescence measurements of the 1,2,4-oxadiazole derivatives were taken with the Andor Solis SR 500i-BL model spectrometer. Signals were collected using Intensified Charge Coupled Device (ICCD) detector camera and the appropriate lenses with 1200 lines/mm grid width at room temperature in the visible region. The samples in the powder form placed at the appropriate angles to the sample holder were excited using the Spectra-Physics model triplet Nd-YLFQ-switch pulse laser with the 349 nm excitation wavelength.

3.3.3 Time-Resolved Fluorescence Spectroscopy

In addition to absorption and fluorescence spectroscopies, which are powerful techniques to get information about the steady-state response of the material after interaction with light, time-resolved fluorescence spectroscopy is used to understand the emission kinetics of fluorescent materials in the excited state.

In the study of this thesis, the lifetime, and the fluorescence emission kinetics of the 1,2,4-oxadiazoles were investigated by using the Picoquant Fluotime 200 system. To excite the materials, a pulsed laser diode having a picosecond pulse width and a wavelength at 375 nm was utilized with a 5 MHz repetition rate, and the emitted photons by the materials were collected as a function of time by using the time-correlated single photon counting (TCSPC) technique. All measurements were carried out at room temperature. On the other hand, analyzing the fluorescence decay curves and determining the fluorescence lifetime (τ) is done by using FluoFit Pro software.

3.3.4 Determination of Fluorescence Quantum Yield

The fluorescence (or photoluminescence) quantum yield (PL QY) is defined as the ratio of the emitted photons per absorbed photons by material displaying emission properties (67). It is the characteristic property of the fluorescent material and is directly associated with the efficiency of the radiative pathways between the molecular states.

The PL QY can be categorized into two types according to the measurement methodology, i.e., relative and absolute quantum yield. In the relative PL QY measurements, a comparative study is followed as the methodology. Here, the fluorescence intensity of the material is compared with that of another fluorescent material having a well-known quantum yield (i.e., reference sample). On the other hand, unlike relative QY measurement, the reference sample is not used during the absolute QY measurement. Here, the numbers of absorbed and emitted photons by the fluorescent material are directly measured by using an integrating sphere.

In this thesis, the PL QY measurements of the 1,2,4-oxadiazoles in solution were carried out by using the relative QY method. To this end, here, the Parker-Rees method was utilized for the PL QY calculations as follows (67),

$$QY_s = QY_r \frac{F_s}{F_r} \frac{A_r}{A_s} \frac{n_s}{n_r} \quad (3.2)$$

where *QY* is the quantum yield, *F* is the spectrally integrated number of photons, *A* is the absorbance at the excitation wavelength (i.e., 350 nm), and *n* is the refractive index of the solvent used in measurements. In the equation, the subscript "*s*" and "*r*" denote the studied sample and the reference sample, respectively. During the measurements, the quinine sulfate 0.5 M H_2SO_4 solution was used as the reference fluorescent dye with the well-known QY of 0.55 (68). On the other hand, the PL QY measurements of the 1,2,4-oxadiazole derivatives in solid-state were performed by using the absolute QY method. To this end, Hamamatsu C11347 Absolute PL Quantum Yield Spectrometer was employed.

4. RESULTS AND DISCUSSION

4.1 Structural Properties of 1,2,4-Oxadiazole Derivatives

In this study, we aimed to synthesize styryl-substituted 1,2,4-oxadiazole compounds by using p-substituted amidoximes and cinnamic acid chlorides as starting materials. To the best of our knowledge, some styryl-1,2,4-oxadiazole derivatives are known in literature with the aspect of synthetic manner, however, there is no report related to the photophysical properties of styryl substituted 1,2,4-oxadiazoles. To this end, considering the importance of 1,2,4-oxadiazoles in pharmaceutical and medicinal chemistry plus no notable study existing about photophysical properties, we have focused, in this study, on the synthesis of styryl-substituted 1,2,4-oxadiazole and their photophysical properties.

The synthetic part of the present work consists of 3 basic steps:

I. Synthesis of p-substituted benzamidoximes as one of the major starting compounds.

II. Synthesis of cinnamic acid chlorides as primary starting material.

III. Synthesis of styryl substituted 1,2,4-oxadiazole derivatives.

First, electron-donating and -withdrawing substituted benzamidoximes have been prepared to start from commercially available benzonitrile derivatives. The physical and spectral data of corresponding amidoximes were consistent with the literature data depicted in Table 4.1 (63).

Table 4.1. Physical and spectroscopic data of amidoxime derivatives.

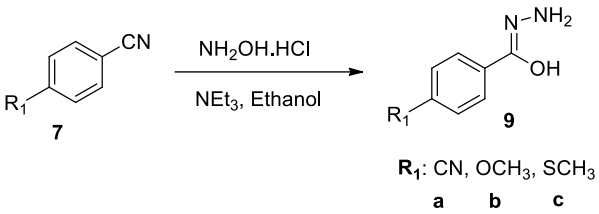

Entry	Compound	R_1	Yield %	Melting point (°C)	IR cm^{-1}
1	9a	CN	75	120-122	3450, 3365 (N−H), 2250 (CN), 1647 (C=N).
2	9b	OCH_3	80	118-119	3443, 3354 (N−H), 1647 (C=N).
3	9c	SCH_3	85	130-131	3497 (N−H), 3234 (broad, NOH, H-bonded), 1655 (C=N)

In the second part of the study, cinnamic acid chlorides, have been obtained by following two sequential steps. According to the literature method described below (64,65), both electron-releasing and -withdrawing substituted aldehydes were reacted with malonic acid in a basic medium to provide cinnamic acids as an intermediate product. Fortunately, these cinnamic acids require no purification steps as they can be easily precipitated from the mother liquor. Further, cinnamic acid was treated with a chlorinating agent to give target cinnamic acid chlorides in excellent yields (90-95%). The structural characterization of **21 a-c** was identified by using physical characteristics and spectroscopic analysis (IR, ^{1}H NMR, and ^{13}C NMR). In the IR spectra of product **21 a-c**, C=O stretching appeared around 1745 cm^{-1}. With the aromatic and olefinic proton signals resonating at around 7.67 and 6.73 ppm, respectively, the structures of **21 a-c** have been proved completely.

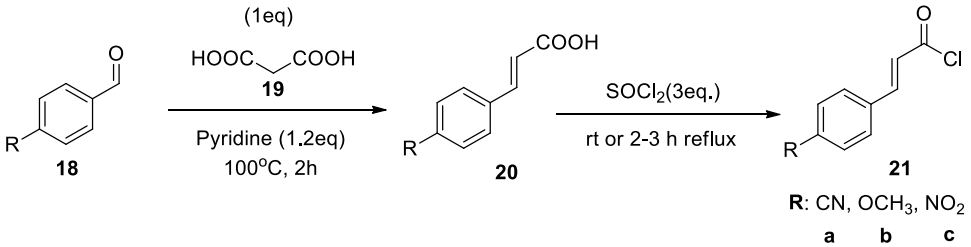

Scheme 4.1. Preparation of cinnamic acid chlorides **21 a-c**.

In the last part, styryl-1,2,4-oxadiazole **23 a-f**, were prepared through the conversion of amidoximes **9** into corresponding acrylamides **22** by cinnamic acid chlorides **21**, then into expected styryl-1,2,4-oxadiazoles **23 a-f** over two steps. Following the current synthetic route, all targeted 1,2,4-oxadiazoles **23 a-f** have been prepared in moderate to good yields (58-68%) (Table 4.2).

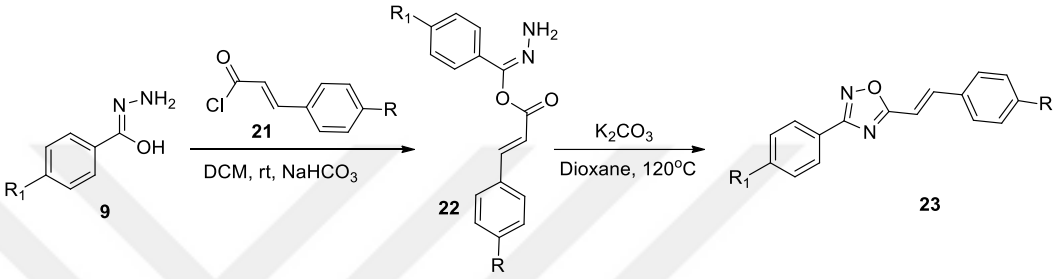

Scheme 4.2. Synthetic pathway for the preparation of styryl-1,2,4-oxadiazole **23a-f**.

Table 4.2. Reaction conditions for the synthesis of styryl-1,2,4-oxadiazoles.

Entry	Product	R	R_1	Temperature (°C)	Time (h)	Yield %
1	23a (RXN-1)	CN	OCH_3	120	12	68
2	23b (RXN-2)	OCH_3	OCH_3	120	12	60
3	23c (RXN-3)	OCH_3	SCH_3	120	12	58
4	23d (RXN-4)	CN	SCH_3	120	12	67
5	23e (RXN-5)	OCH_3	CN	120	12	65
6	23f (RXN-6)	NO_2	CN	120	12	62

The title 1,2,4-oxadiazole **23 a-f** was purified by column chromatography and characterized primarily with IR. Infrared spectra of 23 exhibited characteristic peaks of C=C and C=N at around 1531-1538 cm^{-1}, and 1650-1597 cm^{-1}, respectively. These IR data proved the formation of expected products and were also consistent with the literature values (see Table 4.3).

Table 4.3. Principal IR and NMR data for styryl-1,2,4-oxadiazoles **23**.

Compound	**IR (ν_{max} cm^{-1})**		**^{1}H NMR (δ, ppm)**	**^{13}C NMR (δ, ppm)**	
23	C=C	C=N	Styryl CH	C=N	C=N
23a (RXN-1)	1537	1643, 1607	7.87, 7.16	174.21	168.78
23b (RXN-2)	1536	1644, 1600	7.80, 6.90	175.29	168.26
23c (RXN-3)	1535	1638, 1598	7.85, 6.96	175.52	168.25
23d (RXN-4)	1531	1650, 1601	7.86, 7.15	174.27	168.60
23e (RXN-5)	1538	1631, 1599	7.88, 6.94	176.50	167.49
23f (RXN-6)	1537	1637, 1597	7.91, 7.19	174.35	168.86

Also, relevant styrylic protons (=CH) resonated at around 7.91-6.90 ppm, and the coupling constant of each corresponding proton was found at around J=16.0 Hz in ^{1}H NMR spectra. This result proved that the group attached on a double bond positioned at the opposite side (trans to each other). Moreover, the C-1 and C-2 carbon signals resonated at around 174.21-176.50 and 167.49-168.86 ppm in the ^{13}C-NMR spectra were also supportive data for the formation of expected styryl-1,2,4-oxadiazoles 23 (Table 4.3).

The details of principal ^{1}H- and ^{13}C-NMR chemical shifts of compound 23a (i.e., RXN-1) are given in Figures 4.1 and 4.2 as examples. The structures of all styryl-1,2,4- oxadiazoles 23 were characterized regarding the principal ^{1}H- and ^{13}C-NMR chemical shifts given in Table 4.3.

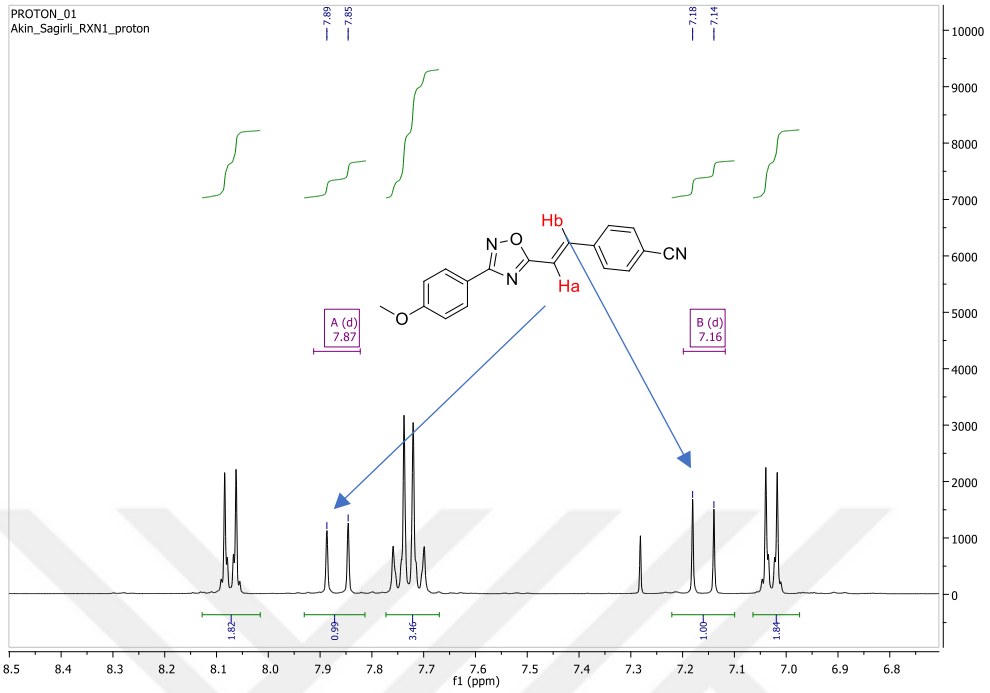

Figure 4.1. Expanded ^{1}H NMR spectrum of compound 23a (i.e., RXN-1).

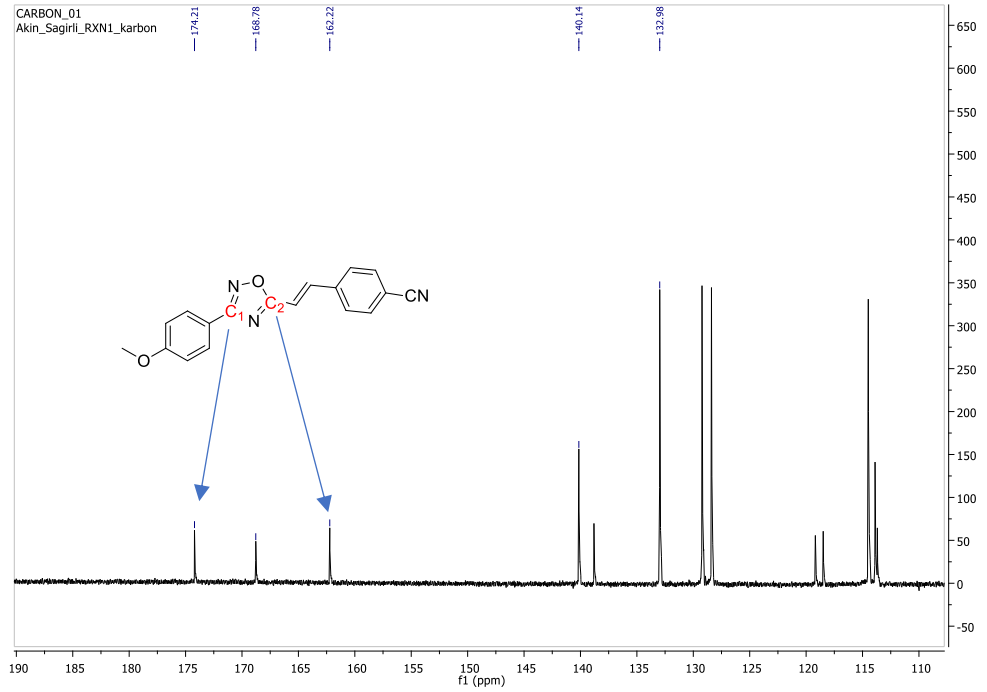

Figure 4.2. Expanded ^{13}C NMR spectrum of compound 23a (RXN-1).

4.2 Photophysical Properties of 1,2,4-Oxadiazole Derivatives

In this section, the photophysical properties of the 1,2,4-oxadiazoles comprising different ED and EW groups on the aryl and styryl moieties, which are investigated by UV-Vis absorption, steady-state and time-resolved fluorescence spectroscopy techniques, are presented. Here in after, the compounds labeled as 23a-23f in the previous sections, will be mentioned as RXN-1-RXN-6, respectively.

4.2.1 UV-Vis Absorption Measurements

UV-Vis absorption spectroscopy was utilized to investigate the photophysical properties of the synthesized 1,2,4-oxadiazole derivatives. The absorption measurements were performed in toluene (C_7H_8) at 0.01 μM of their concentrations and room temperature. Figure 4.3 depicts the absorption spectra of the 1,2,4-oxadiazole derivatives with their molar extinction coefficient or molar absorptivity (ε) and spectral position at maximum absorption.

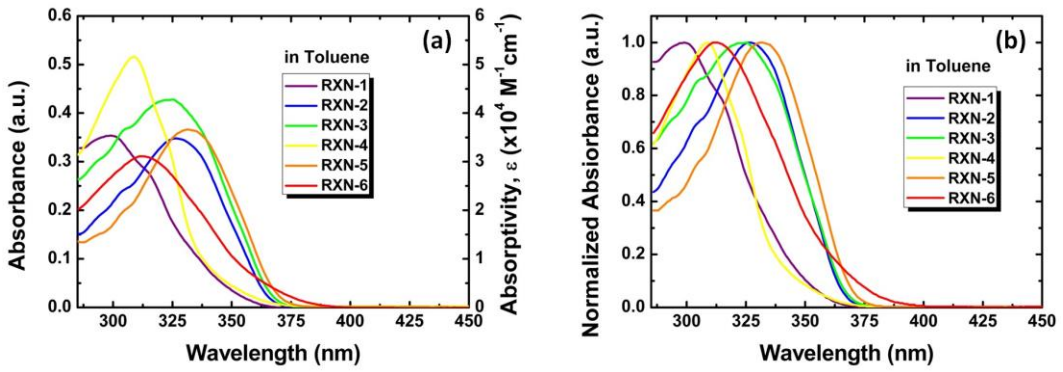

Figure 4.3. UV–Vis absorption spectra of the 1,2,4-oxadiazole derivatives in toluene. (a) The absorbance and the molar extinction coefficients (ε) of the 1,2,4-oxadiazole derivatives and (b) the normalized version of the same absorption curves to see the change in spectral position. All these measurements were carried out at 10^{-5} M of concentration and room temperature.

Although each compound exhibits an almost similar absorption profile, as can be seen in Figure 4.3a, the spectral position of the maximum absorption band and the molar absorptivity are changed depending on the attached ED and EW groups on the aryl and the styryl moieties. The absorption maximum of the compound RXN-1, having -OCH_3 as the ED group on the aryl- and -CN as the EW

group on the styryl-moiety appears on the low wavelength side (i.e., high energy side) of the spectrum at 299 nm (4.15 eV). However, the spectral position of the absorption maxima exhibits 33 nm of redshift, which is the highest with respect to that of RXN-1, when -OCH_3 and -CN groups on the aryl and the styryl moieties are positioned vice versa (i.e., RXN-5). Even though the reverse positioning of the ED and EW groups on the core structure gives rise to a significant spectral change in the position of the absorption band, the molar absorptivity of these compounds remains almost the same. On the other hand, when the -OCH_3 group on the aryl-moiety of the RXN-1 is changed with the thiomethyl (i.e., -SCH_3) that is another electron-donating group, the molar absorptivity of the compound (i.e., RXN-4) exhibits an increment about 45.8% accompanied with a bathochromic shift of 10 nm in the spectral position of the absorption band compared to those of the RXN-1. With this increment, also, the RXN-4 comes up as a compound having the highest molar absorptivity among those of others synthesized in this study. In addition, a compound was designed in the structure including electron-withdrawing groups on both the aryl and styryl moieties in order to analyze the effect of the electron-withdrawing group on the styryl-moiety of the 1,2,4-oxadiazole (i.e., RXN-6). Here, the group of -CN as an electron-withdrawing group was located on the aryl-moiety of the RXN-6 like in the compound RXN-5, while the nitro (-NO_2), another strong electron-withdrawing group, was attached to the styryl-moiety. As compared to the ground-state photophysical properties of the RXN-6 with those of the RXN-5, it exhibits a hypsochromic shift with a decreasing molar absorptivity. The molar absorptivity in Toluene for the RXN-6 was determined as 3.11×10^4 $M^{-1}cm^{-1}$, which is the lowest value among those of all other 1,2,4-oxadiazoles studied here.

To understand the influence of the electron-donating ability of the functional group attached to the aryl-moiety, two different 1.2.4-oxadiazoles were also designed, labeled as RXN-2 and RXN-3. The compounds RXN-2 and RXN-3 have methoxy (-OCH_3) and thiomethyl (-SCH_3) groups on their aryl-moieties, respectively, while both have -OCH_3 group on the styryl-moiety. The absorption maxima for both compounds emerge nearly at the same spectral position (i.e., 328 nm for the RXN-2 and 325 nm for the RXN-3). However, it was found that the absorptivity of the compound exhibits 18.7% of enhancement in the presence of the aryl-moiety bearing the -SCH_3 group. All these findings reveal that the type of

substituent (i.e., electron-donating or -withdrawing group) and their position on the molecule (i.e., aryl- or styryl-moiety) strongly affect the absorption properties of the studied 1,2,4-oxadiazoles, here.

Table 4.4. The ground-state photophysical properties of the 1,2,4-oxadiazoles. $E_T(30)$, λ_{abs}, ε, -R, -R^1, and R-Φ-R^1 are the solvent polarity parameter, wavelength at absorption maxima, molar absorption coefficient, the substituent on aryl-moiety, the substituent on styryl-moiety, and the general representative structure of the 1,2,4-oxadiazole derivatives in terms of ED and EW groups, respectively.

Sample	Solvent	$E_T(30)$ (kcal/mol)	λ_{abs} (nm)	ε (x10^4 $M^{-1}cm^{-1}$)	-R	-R^1	Structure R-Φ-R^1
	Toluene	33.9	299	3.54			
RXN-1	Chloroform	39.1	298	4.21	-OCH_3	-CN	ED-Φ-EW
	1,2-DCE	41.3	297	4.33			
	Toluene	33.9	328	3.48			
RXN-2	Chloroform	39.1	328	3.79	-OCH_3	-OCH_3	ED-Φ-ED
	1,2-DCE	41.3	327	3.55			
	Toluene	33.9	325	4.28			
RXN-3	Chloroform	39.1	325	4.09	-SCH_3	-OCH_3	ED-Φ-ED
	1,2-DCE	41.3	325	3.97			
	Toluene	33.9	309	5.16			
RXN-4	Chloroform	39.1	307	6.00	-SCH_3	-CN	ED-Φ-EW
	1,2-DCE	41.3	307	5.55			
	Toluene	33.9	332	3.66			
RXN-5	Chloroform	39.1	332	3.33	-CN	-OCH_3	EW-Φ-ED
	1,2-DCE	41.3	332	3.33			
	Toluene	33.9	313	3.11			
RXN-6	Chloroform	39.1	314	3.46	-CN	-NO_2	EW-Φ-EW
	1,2-DCE	41.3	313	3.81			

To investigate the effect of the polarity of the medium on the absorption properties of the 1,2,4-oxadiazole derivatives, the UV-Vis absorption measurements were also carried out in solvent mediums having different polarities. Here, chloroform and 1,2-dichloroethane were utilized in the measurements as a solvent medium apart from toluene. The solvent polarities and the results are also summarized in Table 4.4.

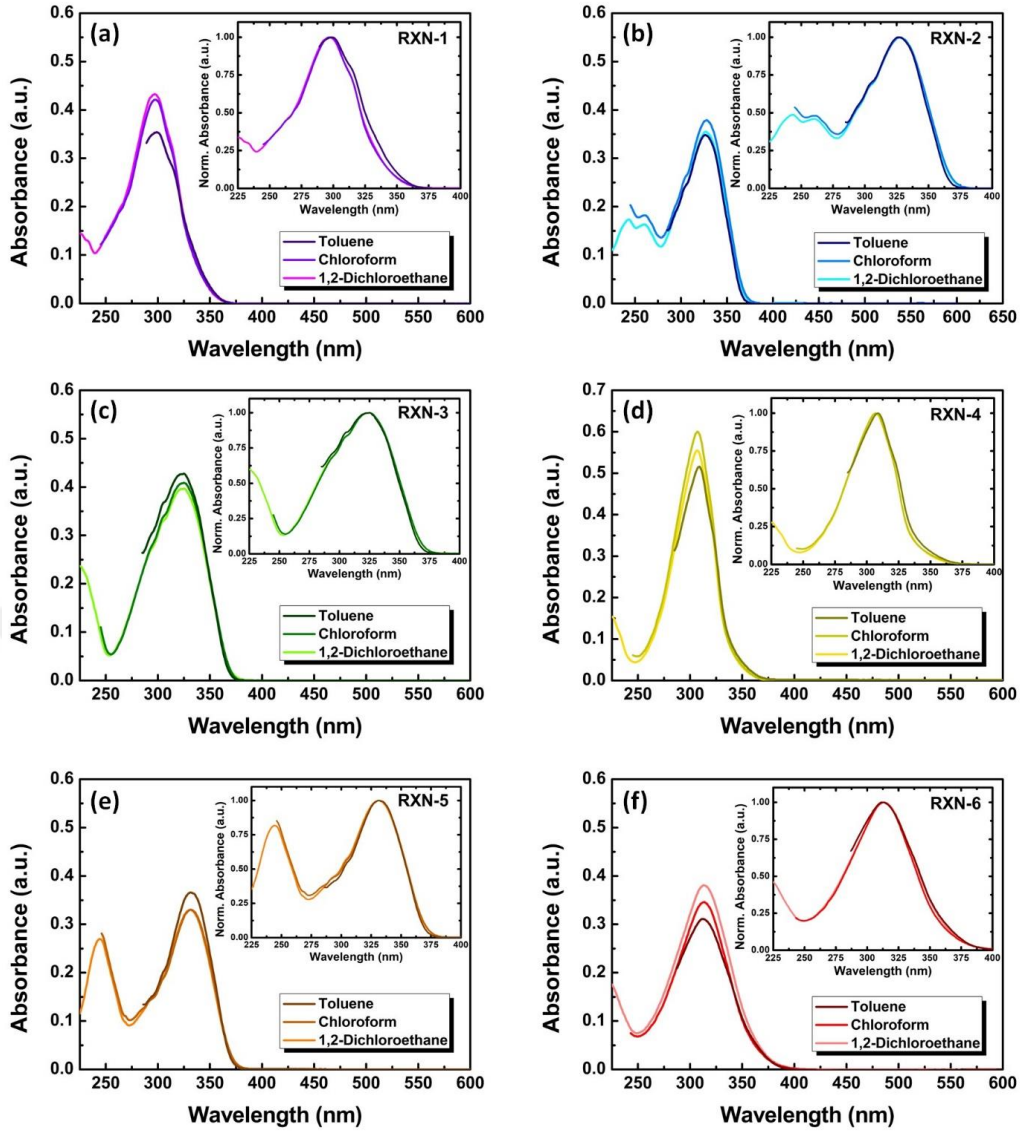

Figure 4.4. UV–Vis absorption measurements of the 1,2,4-oxadiazole derivatives performed in different solvent media such as toluene, chloroform, and 1,2-dichloroethane for (a) RXN-1, (b) RXN-2, (c) RXN-3, (d) RXN-4, (e) RXN-5, and (f) RXN-6. All measurements were carried out at 10^{-5} M of concentration and room temperature. The insets show the zoom-in of the normalized absorption curves.

Figure 4.4 shows the UV-Vis absorption curves recorded in different solvent media at 0.01 μM of their concentrations and the room temperature for the 1,2,4-oxadiazole derivatives. Every solvent has a well-defined wavelength, the so-called UV cutoff, and it absorbs all UV light under this wavelength. Hence, the UV-Vis spectra taken in toluene and chloroform media for all 1,2,4-oxadiazole derivatives could not be shown in the full spectrum frame due to the solvent UV cutoff (see Figure 4.4). As can be seen in the insets of Figure 4.4, all compounds exhibit nearly

solvent-polarity-independent behavior. It was found that the spectral position (i.e., max. 2 nm shift) and the shape of the absorption band remain almost unchanged with the increasing solvent polarity. This indicates that the ground-state properties of the compounds (i.e., structurally, and electronically) are not affected substantially by the change in the polarity of the surrounding medium (69). In addition, it is clearly seen that a dominant absorption peak located around 275 and 325 nm has appeared for each 1,2,4-oxadiazoles in the absorption spectra, and another extra absorption band between 225 and 275 nm emerges in the spectrum of the RXN-5 (see Figure 4.4e). On the other hand, no general behavior was found in the molar absorptivity of the 1,2,4-oxadiazole derivatives with changing solvent polarity. For instance, it is observed an increasing trend in their molar absorptivity for the compounds RXN-1 and RXN-6 with the increasing solvent polarity, whereas the compounds RXN-3 and RXN-5 exhibit a decreasing behavior.

The findings about the photophysical properties of the 1,2,4-oxadiazole derivatives based on the UV-Vis absorption measurements can be summarized item by item as follow:

- Compared the RXN-1 to the RXN-2, it was found that the type of substituent (i.e., electron-donating or electron-withdrawing group) on the styryl-moiety of the compound gives rise to the redshift in the spectral position of the absorption band and dramatically affects the amount of the shift (~29 nm). However, it does not affect the absorbance.
- Compared the RXN-2 to the RXN-5, it was observed that the type of substituent on the aryl-moiety does not significantly affect the spectral position of the absorption band. The electron-withdrawing group causes a small blueshift (~4 nm) and a slight decrease (~5 %) in the molar absorptivity compared to the electron-donating one.
- Compared the RXN-1 to the RXN-4 (or RXN-2 to RXN-3), it was determined that the electron-donating ability of the functional group attached to the aryl-moiety significantly affect the molar absorptivity of the compound. The strong electron-donating group gives rise to an increase in the molar absorptivity (e.g., ~23.0 and 45.8%).

- Compared the RXN-6 to the RXN-5, it was found that the type of substituent on the styryl-moiety significantly affects the spectral position of the absorption band when the group on the aryl-moiety is being an electron-withdrawing one. The electron-withdrawing group on the styryl-moiety leads to a hypsochromic shift in the absorption band (~19 nm) and a decrease in the molar absorptivity (~15 %).
- The polarity of the medium surrounding the compounds almost does not pave the way for a change in the spectral position of the absorption band, whereas it has a slight effect on the molar absorptivity of the compounds.

4.2.2 Computational Study

To better analyze the ground-state photophysical properties of the 1,2,4-oxadiazole derivatives, the quantum chemical computational study comprising was performed by using density functional theory (DFT) (70) via Gaussian 09W software (71). In this study, the calculations such as optimization, vibrational frequencies, and vertical excitation energy for the simulated geometries of all compounds were carried out utilizing the hybrid, nonlocal exchange and correlation functional of Becke-Lee, Parr, and Yang (B3LYP) with the 6-311G(d,p) basis set (72,73). To confirm the optimized geometry of all compounds, the vibrational frequencies were also checked and found to be all positive.

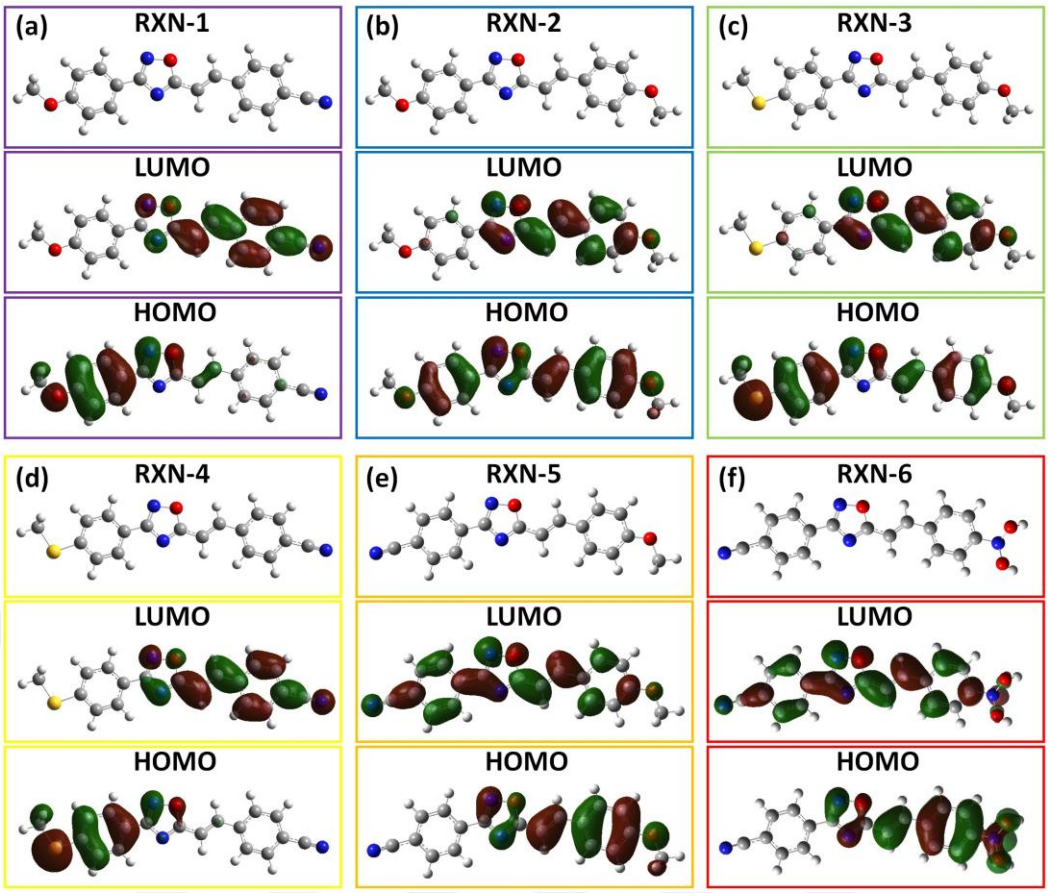

Figure 4.5. The localizations of frontier molecular orbitals (i.e., HOMO and LUMO) on the optimized structures of (a) RXN-1, (b) RXN-2, (c) RXN-3, (d) RXN-4, (e) RXN-5, and (f) RXN-6. In the diagrams, the spheres in red, blue, yellow, grey, and white stand for oxygen, nitrogen, sulfur, carbon, and hydrogen atoms, respectively. The greenish and reddish colors on the molecular diagrams represent the phase of the orbital wave function that are negative and positive, respectively. Toluene was selected as a solvent medium during the calculations.

Figure 4.5 shows the optimized geometries of the 1,2,4-oxadiazole derivatives. The localizations of the frontier molecular orbitals (MO), which are the highest occupied molecular orbital (HOMO) and the lowest unoccupied molecular orbital (LUMO) on the optimized structures, are also given in the Figure. Here, toluene was chosen as a solvent medium during the calculations. As the MO diagrams of RXN-1 and RXN-4 are analyzed, it is clearly seen that the HOMO density is mainly localized on the aryl-moiety having an electron-donating property due to the -OCH_3 and -SCH_3 groups, and partially distributed on the oxadiazole ring. However, the LUMO spreads over the oxadiazole ring and styryl-moiety that have electron-withdrawing properties due to -CN group. It is well known that the ionization

potential and the electron affinity of a molecule are related to its HOMO and LUMO states, respectively. Therefore, the structures with HOMO and LUMO densities mainly localized on the donor and the acceptor moieties, respectively, are preferred to get an efficient charge-separated state by photoexcitation. Hence, the HOMO and LUMO distributions on the structures of the RXN-1 and RXN-4 indicate their intramolecular charge transfer (ICT) characteristics (see Figures 4.5a and 4.5d). In the case of RXN-2 and RXN-3 compounds, it is observed that the HOMO density spreads over the entire backbone due to the presence of electron-donating groups on both the aryl and styryl moieties. The LUMO is localized on the oxadiazole ring with the styryl-moiety of the molecule for both. On the other hand, the vice versa case was observed for the RXN-5 and RXN-6. In the RXN-5, the location of the HOMO density on the molecule shifts toward the styryl-moiety owing to the exchange of the electron-donating and -withdrawing groups positionally in each other as compared to the RXN-1, whereas the LUMO is in the location spread over the whole structure by photo-absorption. In addition, a similar HOMO to LUMO localizations was found for RXN-6 in the presence of electron-withdrawing groups (-CN and -NO_2) on both the aryl and styryl moieties. Here, due to the strong electron-withdrawing property of the -NO_2 group, the 1,2,4-oxadiazole ring can act as an electron-donating group although it has the electron-withdrawing effect, hence, the HOMO can be localized on the side of the styryl-moiety. The findings indicate the intramolecular charge transfer properties of 1,2,4-oxadiazoles can be efficiently modulated by the type and the position of the substituents.

In addition, to obtain the simulated absorption spectra and the corresponding oscillator strengths, the theoretical calculations were carried out by using time-dependent density functional theory (TD-DFT) for the first 12 singlet excited states. Here, toluene was used as a solvent medium in all calculations. Figure 4.6 depicts the absorption spectra with corresponding oscillator strengths obtained for 2,4-oxadiazol derivatives. The calculated transitional properties of all compounds, such as excitation energy, oscillator strength, and absorption wavelength, are also listed in Table 4.5 for the electronic transitions having the first two highest oscillator strengths.

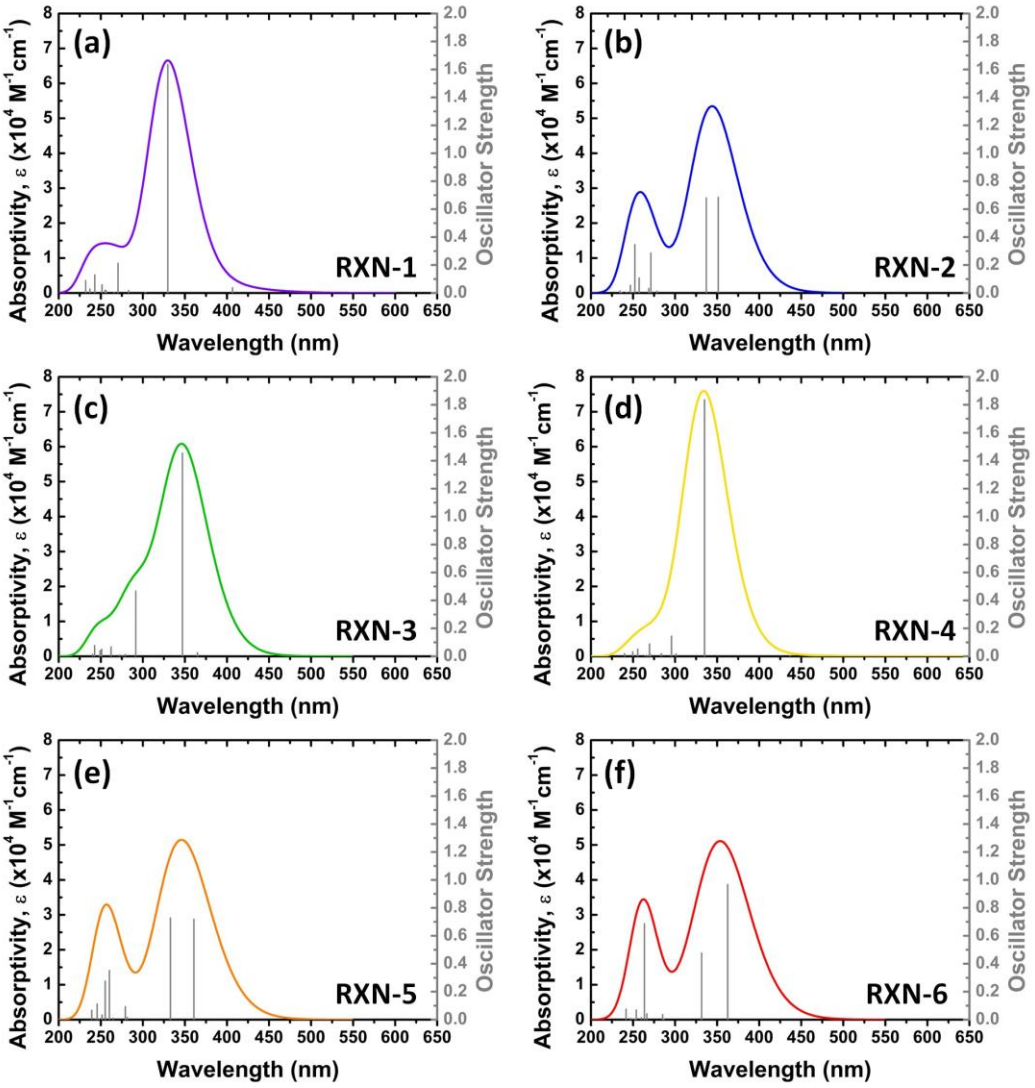

Figure 4.6. The simulated UV–Vis absorption curves of the 1,2,4-oxadiazoles of (a) RXN-1, (b) RXN-2, (c) RXN-3, (d) RXN-4, (e) RXN-5, and (f) RXN-6 by using TD-DFT theory with B3LYP functional and the 6-311G(d,p) basis set. The gray vertical lines also depict the calculated oscillator strength of the electronic states.

As can be seen in Figure 4.6, the stimulated absorption curves exhibit similar evolutionary behavior as compared to those in the experimental ones. For instance, an almost single and narrow absorption band was found for the RXN-4, whereas a broad-waved band (i.e., two absorption peaks) was obtained for the RXN-5. There are two possible transitions (i.e., $\pi \rightarrow \pi^*$ and $n \rightarrow \pi^*$), which can be responsible for the absorption bands in the UV-Vis region. Here, *n*, π, and π* represent the non-bonding orbital, π-bonding orbital, and anti-bonding π orbital, respectively. To better understand the evolution of the absorption spectra in terms of the types and the positions of the substituents, the calculated electronic transitions, and the

oscillator strengths were analyzed for the 1,2,4-oxadiazole derivatives. In the case of the structures with electron-donating and -withdrawing groups on the aryl and styryl moieties, respectively (i.e., RXN-1 and RXN-4), the electronic transition associated with the dominant absorption band was found to be from the ground-state (S_0) to the second excited-state (S_2). The absorption bands appear around 329.74 and 335.03 nm for the RXN-1 and RXN-4, respectively, with the high oscillator strength indicative of the π–π* transition (see Figures 4.6a and 4.6d). In addition, the calculations confirm that the transition from HOMO-1 to LUMO is the major molecular transition, which confirms the π–π* property of the dominant absorption bands both in the spectra of the RXN-1 and RXN-4 (see Table 4.5). On the other hand, the HOMO to LUMO transition (i.e., n→π*) band calculated at 406.55 and 436.75 nm for the RXN-1 and RXN-4, respectively, was not observed with the low oscillator strength (i.e., 0.0373, and 0.0053, respectively) corresponding to this transition band in the absorption spectra. The n →π* transition is generally less probable than π→π* transition since the lone-pair (i.e., non-bonding) electrons are concentrated in a different region of the three-dimensional space, hence, the π→π* transition appears more intensively in UV-Vis absorption spectra than the n →π* transition. In addition, the high charge separation between the HOMO and LUMO for the RXN-1 and RXN-4 can decrease the transition probability (i.e., low oscillator strength) between these orbitals more. On the lower energy side of the spectrum, it was also observed a less intense shoulder around 250 nm, which is related to the HOMO to LUMO+1 transition at 270.50 and 295.80 nm for the RXN-1 and RXN-4, respectively. In the absorption spectrum of the RXN-3, even though the transition from the HOMO-1 to LUMO (i.e., π-π*) is still the major molecular transition, the absorption band associated with the HOMO to LUMO+1 transition at 291.64 becomes more prominent compared to those of the RXN-1 and RXN-4.

Table 4.5. Calculated excitation energy (E_{ex}), absorption wavelength (λ_{abs}), oscillator strength (*f*), molecular orbital (MO) transitions, and contributions of the MO transitions by using time-dependent density functional theory. Here, the excited states having the first two high oscillator strengths are given for each compound.

Compound	Electronic Transition	λ_{abs} (nm)	Oscillator Strength (*f*)	E_{ex} (eV)	MO coefficient	MO in the transition	Percentage contribution of MO (%)
RXN-1	$S_0 \rightarrow S_2$	329.74	1.6358	3.7600	0.69453	HOMO-1→ LUMO	96.47
					0.10374	HOMO → LUMO+1	2.15
	$S_0 \rightarrow S_5$	270.50	0.2132	4.5835	0.13814	HOMO-3→ LUMO+1	3.82
					0.66316	HOMO → LUMO+1	48.17
					-0.11744	HOMO → LUMO+4	2.76
RXN-2	$S_0 \rightarrow S_1$	351.36	0.6854	3.5287	-0.10399	HOMO-1→ LUMO	2.91
					0.69301	HOMO → LUMO	96.05
	$S_0 \rightarrow S_2$	337.16	0.6806	3.6774	0.69438	HOMO-1→ LUMO	96.43
					0.10232	HOMO → LUMO	2.09
RXN-3	$S_0 \rightarrow S_2$	347.05	1.4543	3.5725	0.67050	HOMO-1→ LUMO	89.91
					-0.18072	HOMO → LUMO	6.53
	$S_0 \rightarrow S_3$	291.64	0.4674	4.2513	0.68159	HOMO → LUMO+1	92.91
RXN-4	$S_0 \rightarrow S_2$	335.03	1.8359	3.7007	0.67311	HOMO-1→ LUMO	90.61
					-0.20597	HOMO → LUMO+1	8.48
	$S_0 \rightarrow S_4$	295.80	0.1443	4.1914	-0.22237	HOMO-2 → LUMO	9.89
					0.19627	HOMO-1 → LUMO	7.70
					0.62530	HOMO → LUMO+1	78.20
RXN-5	$S_0 \rightarrow S_1$	360.72	0.7186	3.4371	0.69916	HOMO → LUMO	97.76
	$S_0 \rightarrow S_2$	332.78	0.7281	3.7257	0.70066	HOMO → LUMO+1	98.18
RXN-6	$S_0 \rightarrow S_1$	362.53	0.9663	3.4200	0.70027	HOMO → LUMO	98.08
	$S_0 \rightarrow S_6$	263.54	0.6862	4.7045	0.22479	HOMO-4 → LUMO	10.11
					-0.32880	HOMO-3 → LUMO	21.62
					0.11212	HOMO-1 → LUMO	2.51
					0.55493	HOMO-1→ LUMO+1	61.59

Looking at the absorption spectra of the RXN-2, RXN-5, and RXN-6, the decrement in the intensity of the dominant absorption peak located around 350 nm was observed. In addition, as the calculated oscillator strength values were analyzed, it was found that the HOMO-LUMO (n→π*) transition exhibited considerable contribution to the evolution of the absorption peak. In the absorption spectrum of the structure comprising -OCH_3 group on both aryl and styryl moieties (i.e., RXN-2), the n→π* transition band appears at 351.36 nm, whereas the π→π* transition is at 337.16 nm. Both transitions have almost the same probabilities (i.e., 0.6854 and 0.6806). However, the highest absorption peak in the longer wavelength side of the spectra was found to be directly associated with the n→π* transition for the compounds comprising the -CN group on the aryl-moiety (i.e., RXN-5 and RXN-6). Here, the HOMO-LUMO around 360 nm and the HOMO-LUMO+1 around 330 nm (n→π*) transitions are responsible for the absorption band, while it is π→π* for the absorption peak having lower intensity at the high energy side of the spectrum. The increasing contribution of the n→π* (i.e., HOMO-LUMO or HOMO-LUMO+1) transition in the absorption might be explained by the overlap in the orbitals on the styryl-moiety.

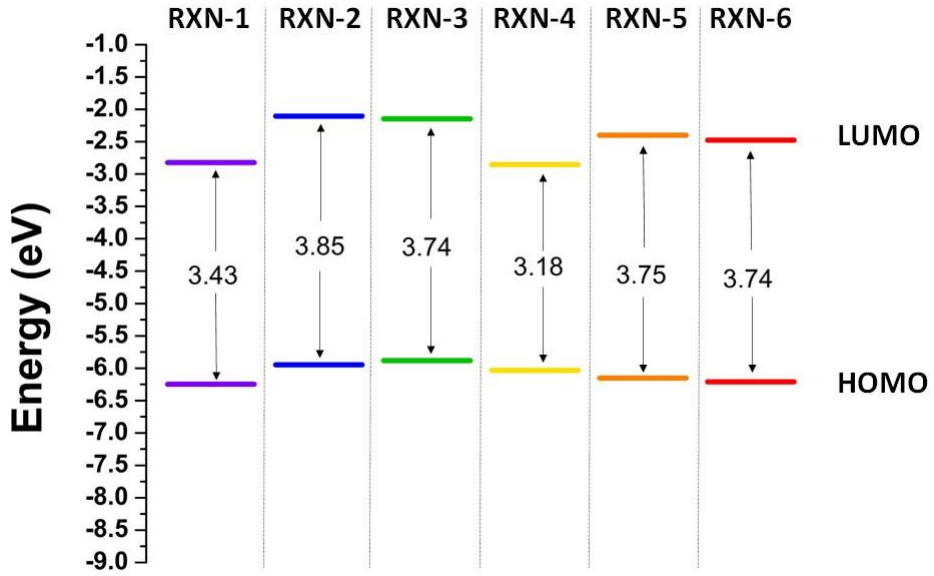

Figure 4.7. The calculated HOMO - LUMO energy levels and energy gaps of the 1,2,4-oxadiazole derivatives in toluene. The energy gap values between the HOMO and LUMO are in the unit of electron-volt (eV).

The energy gap between the HOMO and LUMO was also computed for the 1,2,4-oxadiazole derivatives, and their schematic diagram of the energy levels with the energy gap values is represented in Figure 4.7. As compared the energy levels of the RXN-1 and RXN-4 to those of the RXN-2 and RXN-3, respectively, it is seen that both HOMO and LUMO levels decrease in the case of the electron-withdrawing group (-CN) on the styryl-moiety, instead of the electron-donating groups (-OCH_3 and -SCH_3). In addition, the RXN-1 and RXN-4 have the lowest energy gap values among others due to the fact that their LUMO levels are affected more dramatically than those of the HOMO. On the other hand, it was found the presence of the electron-withdrawing group (-CN), instead of the electron-donating one, on the aryl-moiety leads to a slight decrease in the level of both HOMO and LUMO. Furthermore, it was found that the electron-donating property of the group attached to the aryl-moiety strongly gives rise to a change in the level of HOMO energy. As compared the HOMO level of the RXN-1 to that of the RXN-4, the HOMO is increased with the strong electron-donating group resulting in a decrease in the energy gap. The results suggest that the HOMO-LUMO levels and the energy gap are affected by the type and the position of the substituents. Besides, it can be said that the structure comprising the electron-donating group on the aryl-moiety and the electron-withdrawing group on the styryl-moiety might be preferable to get a better-conjugated system as the significant decrease in energy gap is taken into account.

4.2.3 Steady-State Fluorescence Measurements

The steady-state fluorescence measurements were performed to investigate the excited state photophysical properties of the synthesized 1,2,4-oxadiazole derivatives in this study. During the measurements, the concentration of the prepared solution for each compound was kept in a very dilute case (i.e., 0.01 μM) to prevent the inner filtering effect arising from the strong absorption (i.e., reabsorption effect). In addition, all measurements were done at room temperature and under 350 nm (i.e., 3.54 eV) excitation. The measurements have shown that

two of the synthesized compounds (i.e., RXN-1 and RXN-4) display fluorescence properties in their dilute solutions, while the others do not.

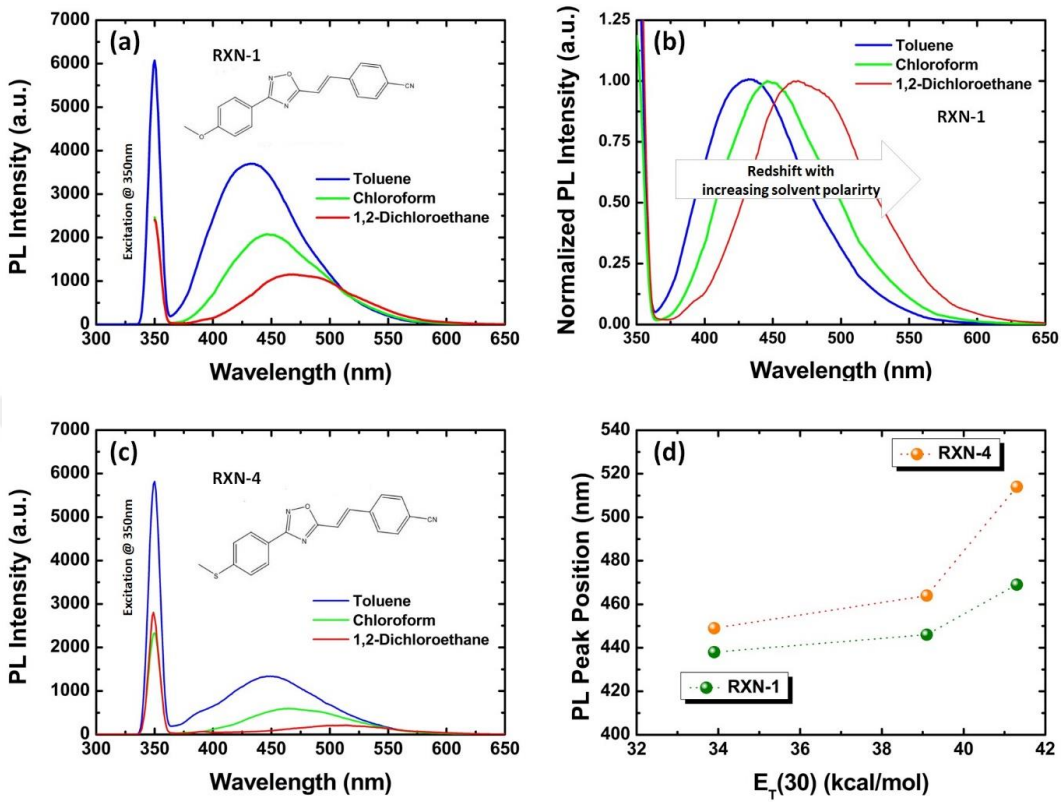

Figure 4.8. The steady-state fluorescence measurements of the 1,2,4-oxadiazole derivatives for (a) RXN-1, and (c) RXN-4 in different solvent mediums such as toluene, chloroform, and 1,2-dichloroethane. (b) The normalized fluorescence emission curves of RXN-1 in different solvent mediums. (d) The change in the peak position of fluorescence emission as a function of solvent polarity. $E_T(30)$ is the solvent polarity parameter.

Figure 4.8 depicts the fluorescence emission curves of the RXN-1 and RXN-4, and their solvent polarity-dependent emission characteristics. It is seen from Figures 4.8a and 4.8c, the fluorescence emission peak emerges at 438 nm for the RXN-1 in toluene, whereas it is at 449 nm for the RXN-4. The shift of about 11 nm toward the longer wavelength of the electromagnetic spectrum reveals that the electron-donating ability of the group located on the aryl-moiety tune the spectral position of the fluorescence emission. This suggests that the stronger electron-donating $-SCH_3$ compared to the $-OCH_3$ lowers the energy gap between the HOMO

and LUMO levels, which is consistent with the theoretical results presented before. On the other hand, it was observed that the fluorescence emission disappeared when the electron-donating group on the aryl-moiety exchanged with the electron-withdrawing group on the styryl-moiety (i.e., RXN-1 and RXN-5). A similar effect was also observed in the case of the RXN-2 and RXN-3. The presence of an electron-donating group on both aryl- and style-moiety gives rise to killing the fluorescence emission. All these findings reveal that the structure comprising the electron-donating group on the aryl-moiety located at the 3-position of the oxadiazole ring and the electron-withdrawing group on the styryl-moiety located at the 5-position might be preferable to get fluorescence emission.

To analyze the effect of the medium surrounding the molecules on the evolution of fluorescence emission, the measurements were also repeated for solvents having different polarities. To this end, chloroform and 1,2-dichloroethane, which have high polarity compared to toluene, were used in the measurements. The measurements reveal that both compounds display significant solvent polarity-dependent emission features. It can be seen in Figures 4.8a and 4.8c that the fluorescence emission intensity is decreased with increasing solvent polarity for both RXN-1 and RXN-4. The decrease in the emission intensity can be attributed to the change in the radiative and nonradiative decay rates in the fluorescence emission kinetics (74). Furthermore, it was found that the spectral position of the fluorescence emission was significantly affected by the solvent polarity, although almost no change was observed in the absorption spectra for both compounds (see Figures 4.4a and 4.4d). Figure 4.8d depicts the change in the peak wavelength of the emission as a function of solvent polarity. Both compounds exhibit a shift to the longer wavelength in their fluorescence spectra (i.e., bathochromic shift) with the increasing solvent polarity. This can be explained by the intermolecular interactions such as hydrogen bonds and dipole-dipole interactions between the solute and solvent molecules (66). It is well-known that aprotic solvents cannot make hydrogen bonding, hence, here, the redshift in the fluorescence emission can be attributed to dipole-dipole interactions. The results also indicate a bigger dipole moment in the excited state (μ_e) compared to that in the ground state (μ_g) for both compounds. The difference between me and mg is directly related to the

redistribution of the charge separation on the molecular structure (i.e., intermolecular charge transfer, ICT), which is consistent with the calculated HOMO and LUMO distributions for the RXN-1 and RXN-4 (see Figures 4.5a and 4.5d). The dipole-dipole interactions between the solute and solvent molecules give rise to a rotational rearrangement in the solvent molecules surrounding solute molecules. The reorientation in the solvent molecules results in a reduction in the excited state energy of the solute molecule, which paves the way for a redshift in the fluorescence emission. In conclusion, increasing the solvent polarity gives rise to a larger redshift in the emission spectrum (75,76).

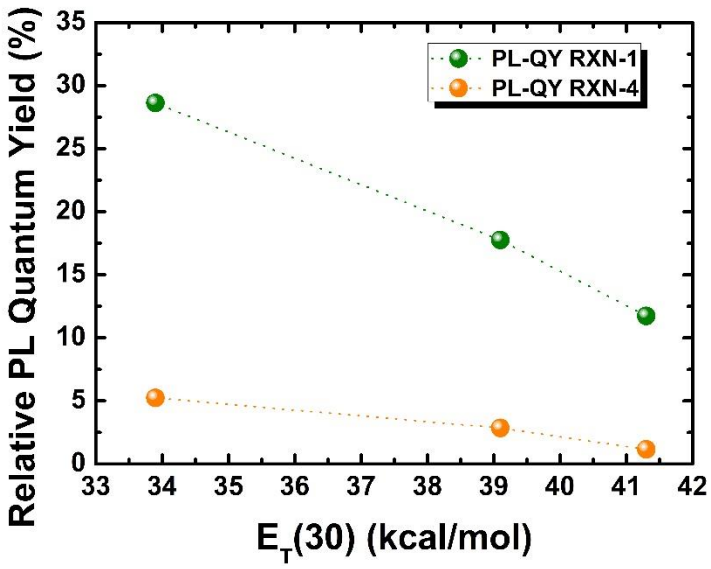

Figure 4.9. Evolution of relative fluorescence quantum yield (PL QY) for the RXN-1 and RXN-4 as a function of solvent polarity parameter.

The fluorescence quantum yield (PL QY) measurements were also performed to better analyze the effect of solvents having different polarities on the emission properties of the RXN-1 and RXN-4. For the measurements, quinine sulfate solution (in 0.5 M H_2SO_4) was used as a reference dye with the reported QY value of 54.6% in the literature (77–79). The calculated PL QY values of the 1,2,4-oxadiazole derivatives exhibiting fluorescence emission are given in Table.4.6. Figure 4.9 shows the change in the relative PL QY values of the RXN-1 and RXN-4 in the different solvent mediums. It was found that both compounds exhibit decreasing PL QY behavior with increasing solvent polarity. The highest PL QY

value was computed as 28.6% for the RXN-1 in toluene, whereas it was found to be 5.2% for the RXN-4. For the RXN-1, the PL QY value decreased by an amount of 59.0% with the increasing solvent polarity compared to that in toluene (i.e., 11.7% PL QY in 1,2-dichloroethane). On the other hand, the rate of reduction in the PL QY for the RXN-4 was also found to be 77.9% as the polarity of the medium increased. This significant change in PL QY demonstrates the dependence of the emission mechanism of compounds RXN-1 and RXN-4 on solvent polarity, and a possible change in the nonradiative decay rate may be responsible for this decrease in the PL QY. These results also suggest that the compounds, especially RXN-1, can be used as potential fluorescent environment-sensitive probes in applications ranging from biological research to clinical diagnostics.

Table 4.6. Fluorescence emission properties, such as emission spectral peak position, and quantum yield, of the RXN-1 and RXN-4 for the solvents having different polarity.

Sample	Solvent	$E_T(30)$ (kcal/mol)	λ_{PL} (nm)	PL QY (%)	-R	-R^1	Structure R-Φ-R^1
	Toluene	33.9	438	28.62			
RXN-1	Chloroform	39.1	446	17.76	-OCH_3	-CN	ED-Φ-EW
	1,2-DCE	41.3	469	11.73			
	Toluene	33.9	449	5.24			
RXN-4	Chloroform	39.1	464	2.85	-SCH_3	-CN	ED-Φ-EW
	1,2-DCE	41.3	514	1.16			

Solid-state emissions of the synthesized 1,2,4-oxadiazole derivatives were also investigated by using a photoluminescence (PL) measurement setup. All measurements were carried out under 349 nm excitation at room temperature. It was observed that all compounds in powder form have a photoluminescence emission. Figure 4.10a depicts the normalized PL emission curves of the 1,2,4-oxadiazole derivatives in solid-state. It was found that the synthesized compounds exhibit PL emission at wavelengths from 447 to 578 nm, depending on the

substituents on the aryl- and styryl-moiety of their structure. To better analyze the spectral peak position of the emissions, the PL emission curves of the 1,2,4-oxadiazole derivatives in solid-state are also presented in Figures 4.10b-4.10g, individually. It can be seen in Figure 4.10b that the PL emission peak of the compound RNX-1 having a donor-acceptor (i.e., ED-EW) structure was located at 463 nm. As the effect of the electron-donating ability of the substituent on the aryl-moiety was analyzed for the donor-acceptor structure, it was observed that the RXN-4 comprising -SCH_3 instead -OCH_3 on the aryl-moiety exhibited a redshift behavior in the PL emission (i.e., 500 nm). The shift to the longer-wavelength side of the PL emission spectrum with attaching a stronger electron-donating group points out the decrease in the energy gap between HOMO and LUMO. In addition, the RXN-5 has the vice versa structure in the types of the substituents on the aryl and styryl moieties compared to the RXN-1, thereby the PL measurement of the RXN-5 can give information about the effect of the substituent type on the emission profile (Figure 4.10f). The PL emission was found to be significantly affected by the type of substituent and red-shifted about 34 nm compared to that of the RXN-1. On the other hand, when the PL emission features of the compounds having symmetrical structures like donor-donor (i.e., RXN-2 and RXN-3) or acceptor-acceptor (i.e., RXN-6) were analyzed, it was observed a shift to the shorter wavelengths in the case of the RXN-2 and RXN-3, whereas the PL peak position shifted to a longer wavelength in the case of the RXN-6, compared to the PL curve of the RXN-1. The results can be attributed to the charge distributions, where the electron density is spread over the entire structure in the ground state (i.e., HOMO) for the RXN-2 and RXN-3, while it is in the excited state (i.e., LUMO) for the RXN-6.

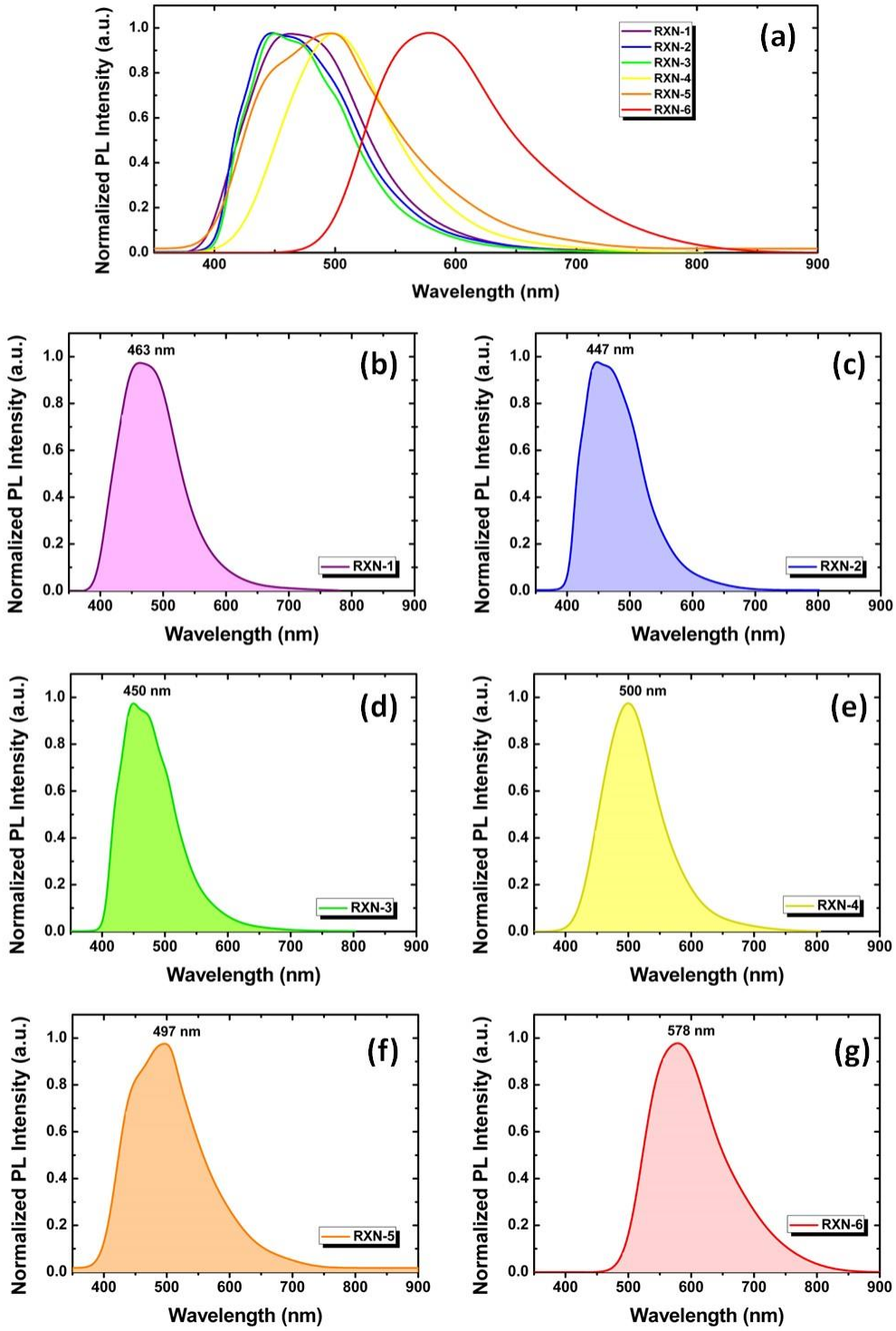

Figure 4.10. The normalized photoluminescence emission curves of the 1,2,4-oxadiazoles given (a) together and (b)-(g) individually.

The absolute PL QY measurements were also done for the compounds in the solid state. The measurements were carried out at room temperature for different excitation wavelengths. The collected PL QY data were summarized in Table 4.7

and plotted in Figure 4.11. As can be seen in the figure, all compounds exhibit almost excitation-wavelength independent PL QY behavior in solid-state. It was observed that compounds having the donor-acceptor structure (RXN-1 and RXN-4) have the highest PL QY compared to those of others. The absolute PL QY was measured as 11.6% under the 350 nm excitation for the RXN-4, whereas it was found to be 10.3% for the RXN-1. This increment in the PL QY can be explained by the higher electron-donating ability of the SCH_3 group instead of the OCH_3 group on the aryl-moiety. It was also found that the presence of the electron-donating group instead the electron-withdrawing group on the styryl-moiety paved the way for a 2-folds decrease in the PL QY (RXN-1 and RXN-2). On the other hand, the electron-withdrawing group attached to the aryl-group exhibits similar behavior in PL QY measurements. The electron-withdrawing group instead electron-donating group on the aryl-moiety causes a decrease of about 12-fold in PL QY (RXN-2 and RXN-5). The results reveal that the presence of the electron-donating group on the styryl-moiety and the electron-withdrawing group on the aryl-moiety promotes the nonradiative decay pathways.

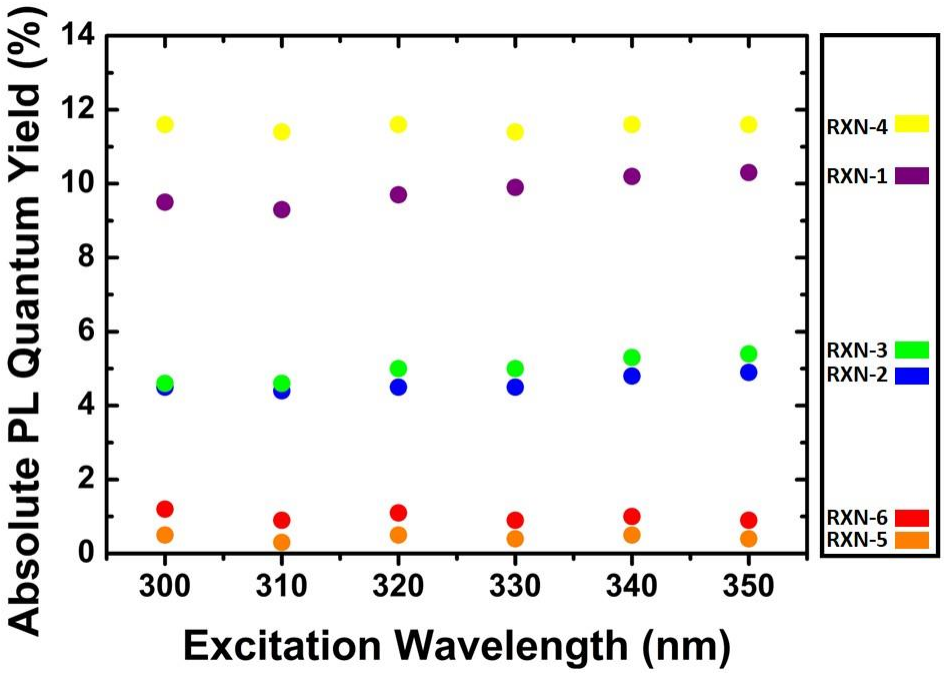

Figure 4.11. The absolute photoluminescence quantum yield measurements of the 1,2,4-oxadiazole derivatives as a function of excitation wavelength.

Table 4.7. Some photophysical properties of the 1,2,4-oxadiazole derivatives in solid-state.

Sample	λ_{PL} (nm)	PL QY @350nm (%)	τ_{av} (ns)	k_r ($x10^7$ s^{-1})	k_{nr} ($x10^7$ s^{-1})	-R	-R^1	Structure R-Φ-R^1
RXN-1	463	10.3	2.21	4.66	40.59	-OCH_3	-CN	ED-Φ-EW
RXN-2	447	4.9	0.90	5.44	105.67	-OCH_3	-OCH_3	ED-Φ-ED
RXN-3	450	5.4	1.38	3.91	68.55	-SCH_3	-OCH_3	ED-Φ-ED
RXN-4	500	11.6	2.97	3.91	29.76	-SCH_3	-CN	ED-Φ-EW
RXN-5	497	0.4	0.70	0.57	142.29	-CN	-OCH_3	EW-Φ-ED
RXN-6	578	0.9	0.74	1.22	133.92	-CN	-NO_2	EW-Φ-EW

4.2.4 Time-Resolved Fluorescence Measurements

The time-resolved fluorescence (TRF) measurements were performed under 375 nm excitation at room temperature to understand the emission kinetics of the 1,2,4-oxadiazole derivatives in solid-state. Figure 4.12 represents the PL decay curves collected at the maximum emission wavelengths (λ_{PL}) of the compounds in the solid-state. As can be seen in the figure, the PL decay curve accelerated when the electron-withdrawing group on the aryl-moiety was changed with the donating one, although it elongated for the compounds in the structure of the donor-acceptor (i.e., RXN-1 and RXN-4). It was also found that the decay curve further sped up by substituting the electron-withdrawing group on the aryl-moiety, instead the electron-donating one (i.e., RXN-5). This gradually accelerated fluorescence decay behavior in the donor-donor (i.e., RXN-2 and RXN-3), acceptor-donor (i.e., RXN-5), and acceptor-acceptor (i.e., RXN-6) structured compounds is well consistent with the results obtained in PL QY measurements for the corresponding compounds, which is the indication of the nonradiative decay pathways become more dominated.

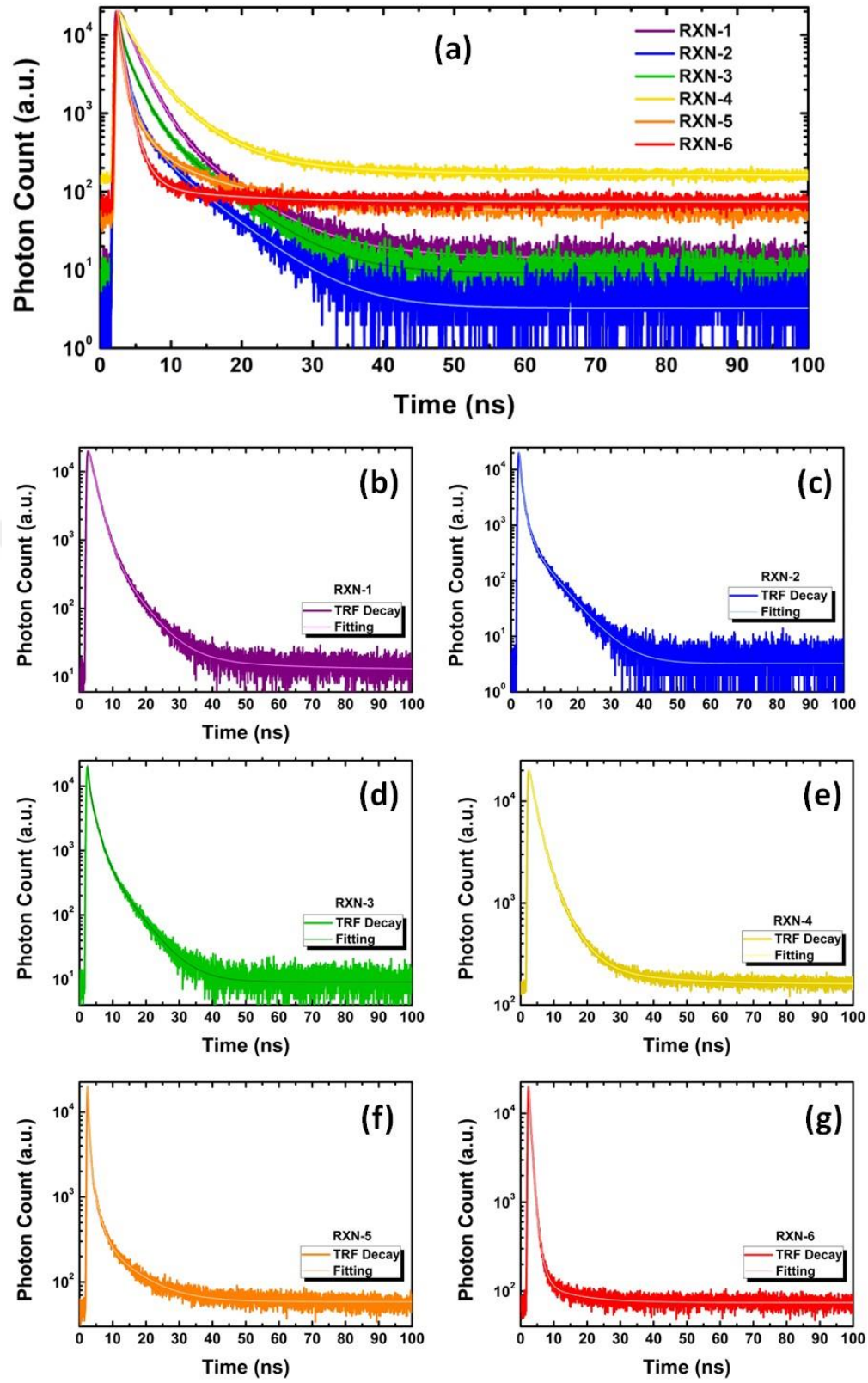

Figure 4.12. Time-resolved fluorescence decay curves of the 1,2,4-oxadiazoles given (a) together and (b)-(g) individually. The solid line inside the decay curves represents the exponential fitting curves.

To analyze the emission kinetics of the compounds the PL decay curves were numerically fitted by using the multi-exponential decay function given as follows (66),

$$I(t) = \sum_{i=1}^{n} A_i \, e^{-\frac{t}{\tau_i}} \quad (4.1)$$

where A is the amplitude of the exponential decay and τ is the fluorescence lifetime. The computed amplitude averaged fluorescence lifetime (τ_{av}) for each compound is given in Table 4.7. It was found that the fluorescence lifetime strongly depends on the substituent type (i.e., ED and EW) and -position (i.e., aryl and styryl moieties) on the compounds. The fluorescence decay lifetime was found to be 2.21 ns for the RXN-1, while it decreased to 0.90 ns when the EW group of CN on the styryl-moiety replaced the ED group of OCH_3 for RXN-2. It was also observed that the fluorescence lifetime further shortened up to 0.70 ns when the OCH_3 on the aryl-moiety was exchanged with the CN on the styryl-moiety (i.e., RXN-5). These results suggest that the presence of an electron-withdrawing group on the aryl-moiety and also an electron-donating group on the styryl-moiety feed the non-radiative processes in the 1,2,4-oxadiazole derivatives. The decrease in the PL QY (see Table 4.7) accompanied by the shortening fluorescence lifetime also reinforce this possible scenario based on the enhancement in non-radiative decay rate. Hence, the radiative and non-radiative decay rates were also calculated by using the equations as follows (66),

$$k_r = \frac{\phi}{\tau} \quad (4.1)$$

and

$$k_{nr} = \frac{(1-\phi)}{\tau} \quad (4.2)$$

where k_r, k_{nr}, ϕ, and τ are the radiative and nonradiative decay rates, fluorescence quantum yield, and lifetime, respectively. During the calculations, the amplitude averaged fluorescence lifetimes (τ_{av}) and absolute PL QY values were utilized for

the 1,2,4-oxadiazoles in solid-state. Figure 4.13 shows the calculated radiative and non-radiative decay rate constants for all compounds in the solid state, which are also summarized in Table 4.7.

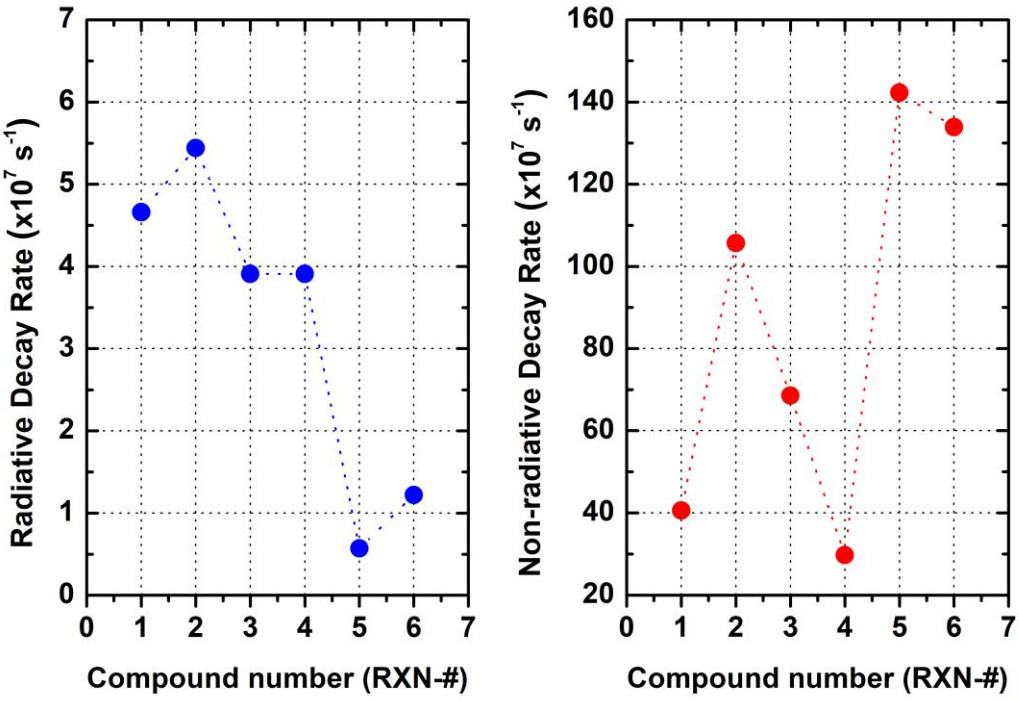

Figure 4.13. Radiative and non-radiative decay rates calculated by using experimental amplitude averaged lifetime and PL QY values for the 1,2,4-oxadiazole derivatives in solid phases. Here, the radiative and non-radiative decay rates are given in blue and red solid circles, respectively.

The radiative decay rate is found to be lowest for the RXN-1 and RX-4 among those of other compounds, it reaches the highest values for the RXN-5 and RXN-6. As the calculated values are examined in detail, it is observed that although the radiative decay rate of the RXN-2 accelerates compared to that of the RXN-1, its PL QY decreases by about 52.4% to that of the RXN-1. However, the non-radiative decay rate of the RXN-2 is found to be increased 2.6-fold compared to RXN-1, explaining the dramatic decrease in the PL QY of the RXN-2 compared with that of the RXN-1. On the other hand, the RXN-4 has the highest PL QY than the RXN-1, even though it has about a 16.1% lower radiative decay rate. However, the non-radiative decay rate, which is about 26.7% lower compared to that of the RXN-1,

explains why the RXN-4 exhibits a higher PL QY than that of the RXN-1. In the case of the RXN-5 and RXN-6, they have the highest non-radiative decay rates among those of the other compounds. They have non-radiative decay rates about 3.5- and 3.3-fold high than that of the RXN-1, respectively. They have non-radiative decay rates about 3.5- and 3.3-fold high than that of the RXN-1, respectively. In addition, their radiative decay rates exhibit a dramatic decrease (see Table 4.7). Both decreases in the radiative decay rate and increases in the non-radiative decay rate result in very low PL QY for the RXN-5 and RXN-6.

5. CONCLUSIONS AND RECOMMENDATIONS

In this thesis, the micro-molecules of 1,2,4-oxadiazoles decorated with different electron-donating and -withdrawing functional groups, such as OCH_3, SCH_3, CN, and NO_2, on the aryl and styryl moieties were successfully synthesized characterized utilizing both NMR and FT-IR spectroscopies. The photophysical properties of the synthesized compounds were also studied by using UV-Vis absorption, steady-state fluorescence, and time-resolved fluorescence spectroscopy techniques. Furthermore, to elucidate the intramolecular charge transfer characteristics of the synthesized compounds, the quantum chemical calculations were performed by utilizing density functional theory with Gaussian 09 software. The experimental studies were conducted for two different phases of the compounds, i.e., in solution and solid state.

The UV-Vis absorption and fluorescence measurements showed that the type of substituent (i.e., electron-donating or -withdrawing group) on the aryl and styryl moieties significantly affects the photophysical properties of the synthesized compounds in their dilute solutions. It was found that the type of substituent (i.e., electron-donating or -withdrawing group) on the aryl- or styryl-moiety gives rise to significant changes both in their spectral position of the absorption band and molar absorptivity. In addition, it was observed that the polarity of the medium surrounding the compound molecules almost does not affect the spectral position of the absorption band, while a slight effect on their molar absorptivity. On the other hand, fluorescence measurements depicted that 1,2,4-oxadiazole derivatives, just comprising the electron-donating group on the aryl-moiety and the electron-withdrawing group on the styryl-moiety, displayed fluorescence emission in solution. The theoretical calculations (i.e., DFT) revealed the strong intramolecular charge transfer property of the donor-acceptor structured 1,2,4-oxadiazole derivatives, which govern their emission properties in solution. It was also found that the fluorescence quantum yield and the spectral position of emission are significantly affected by the polarity of the solvent. Both compounds (RXN-1 and RXN-4) exhibited red-shifted behavior in the fluorescence emission spectrum accompanied by a decreasing trend in their fluorescence quantum yields with increasing solvent polarity. The findings for the fluorescence emission properties

with increasing solvent polarity can be interpreted by a possible change in the non-radiative decay rate, due to the dipole-dipole interactions between the compound molecules having strong intramolecular charge transfer characteristics and the solvent molecules surrounding them.

On the other hand, the photoluminescence measurements showed that the synthesized 1,2,4-oxadiazoles can emit fluorescence emission in the solid-state. To the best of our knowledge, this is the first-time report in the literature for the solid-state fluorescence emission in the micro-molecules of the 1,2,4-oxadiazoles. It was found that the synthesized compounds exhibit PL emission at wavelengths from 447 to 578 nm, depending on the substituents on the aryl- and styryl-moiety of their structure. The compounds comprising the electron-donating group on the aryl-moiety and the electron-withdrawing group on the styryl-moiety (i.e., RXN-1 and RXN-4) were found to have relatively high quantum yields. The time-resolved fluorescence measurements also confirmed this behavior obtained for the fluorescence quantum yield in solid-state. The measurements revealed that the non-radiative decay rate in the emission mechanism of the compounds dominantly governs their fluorescence emission in solid-state, depending on the type of substituent (i.e., electron-donating or -withdrawing group) on the aryl and styryl moieties.

All these findings reveal that 1,2,4-oxadiazoles is a potential candidate as a fluorescent organic material for applications in need of fluorescence emission in solution and/or in solid state. However, it still needs to improve the photophysical properties with the designing of new molecular structures having strong intramolecular charge transfer characteristics.

6. REFERENCES

"Vancouver citation system was used in this thesis."

1. Resch-Genger U, Grabolle M, Cavaliere-Jaricot S, Nitschke R, Nann T. Quantum dots versus organic dyes as fluorescent labels. Nat Methods. 2008;5(9):763–75.

2. Mason WT. Fluorescent and Luminescent Probes for Biological Activity: A Practical Guide to Technology for Quantitative Real-Time Analysis. Elsevier. 1999. 647 p.

3. Jestin Y. Down-shifting of the incident light for photovoltaic applications [Internet]. Vol. 1, Comprehensive Renewable Energy. Elsevier Ltd.; 2012. 563–585 p. Available from: http://dx.doi.org/10.1016/B978-0-08-087872-0.00131-1

4. Slodek A, Matussek M, Filapek M, Szafraniec-gorol G, Maron A, Schab-balcerzak E, et al. Small Donor – Acceptor Molecules Based on a Quinoline – Fluorene System with Promising Photovoltaic Properties.

5. Wang Y, Liu W, Qu Z, Tan H, Liu Y, Xie G. Dyes and Pigments Spirotriphenylamine based star-shaped D-A molecules meeting AIE chromophore for both ef fi cient solution-processed doped and nondoped blue organic light-emitting diodes. Dye Pigment [Internet]. 2017;143:173–82. Available from: http://dx.doi.org/10.1016/j.dyepig.2017.04.030

6. Byeon SY, Choi JM, Lee JY. Dyes and Pigments Pyridoindole based intramolecular charge transfer type host material for blue phosphorescent organic light-emitting diodes. Dye Pigment [Internet]. 2016;134:285–90. Available from: http://dx.doi.org/10.1016/j.dyepig.2016.07.021

7. Bhagwat AA, Mohbiya DR, Avhad KC, Sekar N. Spectrochimica Acta Part A : Molecular and Biomolecular Spectroscopy Viscosity-active D- π -A chromophores derived from benzo [b] thiophen-3 NLO properties. Spectrochim Acta Part A Mol Biomol Spectrosc [Internet]. 2018;203:244–57. Available from: https://doi.org/10.1016/j.saa.2018.05.101

8. Khopkar S, Jachak M, Shankarling G. Viscosity sensitive semisquaraines based on 1 , 1 , 2-trimethyl-1H-benzo [e] indole : Photophysical properties , intramolecular charge transfer , solvatochromism , electrochemical and DFT study. J Mol Liq [Internet]. 2019;285:123–35. Available from: https://doi.org/10.1016/j.molliq.2019.03.173

9. Deshpande SS, Khopkar SS, Shankarling GS. Dyes and Pigments A thiazoloquinoxaline based " turn-on " chemodosimeter for detection of copper ions. Dye Pigment [Internet]. 2017;147:393–9. Available from: http://dx.doi.org/10.1016/j.dyepig.2017.08.037

10. Paun A, Hadade ND, Paraschivescu CC, Matache M. 1,3,4-Oxadiazoles as luminescent materials for organic light emitting diodes via cross-coupling reactions. J Mater Chem C [Internet]. 2016;4:8596–610. Available from: http://dx.doi.org/10.1039/C6TC03003C

11. Pankrateva VE, Sharonova T V, Tarasenko M V, Baikov S V, Kofanov ER. One-Pot Synthesis of 3,5-Disubstituted 1,2,4-Oxadiazoles Using Catalytic System NaOH–DMSO. 2018;54(8):1250–5.

12. Buscemi S, Pace A, Piccionello AP, Vivona N. Synthesis of fluorinated first generation starburst molecules containing a triethanolamine core and 1,2,4-oxadiazoles. 2006;127:1601–5.

13. Parra M, Hidalgo P, Carrasco E, Barberá J, Silvino L. New 1,2,4- and 1,3,4-oxadiazole materials: synthesis, and mesomorphic and luminescence properties. 2006;33:875–82.

14. Li Q, Cui L, Zhong C, Yuan X, Dong S, Jiang Z-Q, et al. Synthesis of new bipolar host materials based on 1,2,4-oxadiazole for blue phosphorescent OLEDs. Dye Pigment [Internet]. 2014;101:142–9. Available from:

http://dx.doi.org/10.1016/j.dyepig.2013.09.029

15. Li Q, Cui L, Zhong C, Jiang Z, Liao L. Asymmetric Design of Bipolar Host Materials with Novel 1,2,4- Oxadiazole Unit in Blue Phosphorescent Device. Org Lett. 2014;16:1622–5.

16. Matta A, Bahadur V, Taniike T, Eycken J Van Der, Singh BK. Synthesis , characterisation and photophysical studies of oxadiazolyl coumarin : A new class of blue light emitting fluorescent dyes. Dye Pigment [Internet]. 2017;140:250–60. Available from: http://dx.doi.org/10.1016/j.dyepig.2017.01.050

17. Hendawy OM. A comprehensive review of recent advances in the biological activities of 1,2,4 - oxadiazoles. 2022;355(7):1–14.

18. Dhameliya TM, Chudasma SJ, Patel TM, Dave BP. A review on synthetic account of 1,2,4 - oxadiazoles as anti - infective agents. Mol Divers [Internet]. 2022;26(5):2967–80. Available from: https://doi.org/10.1007/s11030-021-10375-4

19. Vaidya A, Devender P, Shah K. 1 , 3 , 4-oxadiazole and its derivatives : A review on recent progress in anticancer activities. 2021;97:572–91.

20. Ryan NJ. Ataluren : First Global Approval. 2014;74:1709–14.

21. Stern EP, Host L V, Wanjiku I, Escott KJ, Gilmour PS, Ochiel R, et al. Zibotentan in systemic sclerosis - associated chronic kidney disease : a phase II randomised placebo - controlled trial. Arthritis Res Ther [Internet]. 2022;130:1–13. Available from: https://doi.org/10.1186/s13075-022-02818-6

22. Wang Z, Wang M, Yao X, Li Y, Qiao W, Geng Y, et al. Hydroxyl may not be indispensable for raltegravir : Design , synthesis and SAR Studies of raltegravir derivatives as HIV-1 inhibitors HO. Eur J Med Chem [Internet]. 2012;50:361–9. Available from: http://dx.doi.org/10.1016/j.ejmech.2012.02.015

23. Ningaiah S, Bhadraiah UK, Keshavamurthy S, Javarasetty C. Novel pyrazoline amidoxime and their 1 , 2 , 4-oxadiazole analogues : Synthesis and pharmacological screening. Bioorg Med Chem Lett [Internet]. 2013;23:4532–9. Available from: http://dx.doi.org/10.1016/j.bmcl.2013.06.042

24. Filho MJ, Leite CA, Oliveira B, Moreira M, Lima MS, Soares M, et al. Design, synthesis and cruzain docking of 3-(4-substituted-aryl)-1,2,4- oxadiazole-N-acylhydrazones as anti-Trypanosoma cruzi agents. Bioorg Med Chem [Internet]. 2009;17:6682–91. Available from: http://dx.doi.org/10.1016/j.bmc.2009.07.068

25. Shamsi F, Hasan P, Queen A, Hussain A, Khan P, Zeya B, et al. Synthesis and SAR studies of novel 1,2,4-oxadiazole-sulfonamide based compounds as potential anticancer agents for colorectal cancer therapy. Bioorg Chem [Internet]. 2020;98:103754. Available from: https://doi.org/10.1016/j.bioorg.2020.103754

26. Upare AA, Gadekar PK, Sivaramakrishnan H, Naik N, Khedkar V, Sarkar D, et al. Design, synthesis and biological evaluation of (E) -5-styryl-1,2,4-oxadiazoles as anti-tubercular agents. Bioorg Chem [Internet]. 2019;86:507–12. Available from: https://doi.org/10.1016/j.bioorg.2019.01.054

27. Mayer JCP, Acunha T, Rodrigues OED, Back DF, Chaves OA, Dornelles L, et al. Synthesis, spectroscopic characterization and DNA/HSA binding study of1 (phenyl/naphthyl)ethenyl-substituted 1,3,4-oxadiazolyl-1,2,4-oxadiazoles. New J Chem. 2021;45:471–84.

28. Mayder DM, Tonge CM, Hudson ZM. Thermally Activated Delayed Fluorescence in 1,3,4-Oxadiazoles with π - Extended Donors. J Org Chem. 2020;85:11094–103.

29. Gallardo H, Cristiano R, Vieira AA, Filho RAWN, Srivastava RM, Bechtold IH. Non-symmetrical luminescent 1,2,4 - oxadiazole - based liquid crystals. Liq Cryst. 2008;35(7):857–63.

30. Mohamed MFA, Marzouk AA, Nafady A, El-gamal DA, Allam RM, Abuo-rahma GEA, et al. Design, synthesis and molecular modeling of novel aryl carboximidamides and 3-aryl-1,2,4-oxadiazoles derived from indomethacin as potent anti-inflammatory iNOS / PGE2 inhibitors. Bioorg Chem [Internet]. 2020;105:104439. Available from: https://doi.org/10.1016/j.bioorg.2020.104439

31. Brahmi J, Ghannay S, Bakari S, Aouadi K, Kadri A, Msaddek M, et al. Unprecedented stereoselective synthesis of 3-methylisoxazolidine-5-aryl-1,2,4-oxadiazoles via 1,3-dipolar cycloaddition and study of their in vitro antioxidant activity. Synth Commun [Internet]. 2016;46(24):2037–44. Available from: http://dx.doi.org/10.1080/00397911.2016.1244692

32. Kim J, Shin JS, Ahn S, Han SB, Jung Y. 3-Aryl-1,2,4-oxadiazole Derivatives Active Against Human Rhinovirus. Med Chem Lett. 2018;9:667–72.

33. Pevear DC, Tull TM, Seipel ME, Groarke JM. Activity of Pleconaril against Enteroviruses. Antimicrob Agents Chemother. 1999;43(9):2109–15.

34. Bártfai Z, Somosközi A, Puhó EH, Czeizel AE. No teratogenic effect of prenoxdiazine: A population-based case – control study. Congenit Anom (Kyoto). 2007;47:16–21.

35. Biernacki K, Dasko M, Ciupak O, Kubinski K, Rachon J, Demkowicz S. Novel 1,2,4-Oxadiazole Derivatives in Drug Discovery. Pharmaceuticals. 2020;13(6):111.

36. Witanowski M, Biedrzycka Z, Sicinska W, Grabowski Z, Webb GA. Solvent Effects on the Nitrogen NMR Shieldings in Oxazole and Oxadiazole Systems. J Magn Reson Ser A. 1996;120(2):148–54.

37. Clapp LB. 1,2,4-Oxadiazoles. Adv Heterocycl Chem. 1976;20:65–116.

38. Kurt B.G. Torssell. Nitrile oxides, nitrones, and nitronates in organic synthesis. Berlin: VCH Publishers; 1988.

39. Caramella P, GrMnanger P. Padwa, Albert, ed. 1, 3-Dipolar cycloaddition chemistry. Padwa A, editor. Wiley; 1984. 291 p.

40. Unangst PC, Shrum GP, Connor DT, Dyer RD, Schriert DJ. Novel 1,2,4-Oxadiazeles and 1,2,4-Thiadiazoles as Dual 5-Lipoxygenase and Cyclooxygenase Inhibitors. J Med Chem. 1992;35:3691–8.

41. Bianchi BG, Gandolfi R. 2-lsoxazoline Derivatives. Part V.l Regio- and Stereo-selectivity in the Cycloadditionof BenzonitrileOxideto Some Cycloalkeneand 2-lsoxazoline Derivatives. J Chem Soc Perkin Trans. 1972;1:1711–4.

42. J.-P. Giberl, Petrus C, Petrus F. Competition entre les réactivités dipolarophiles et nucléophiles des pyrazolines-2 dans l'action de l'oxyde de benzonitrile. Synthèse, identification, comportement chimique des tétrahydropyrazolo-[4,5-b] oxadiazoles-1,2,4. J Heterocycl Chem. 1979;16(2):311–20.

43. Hemming K. Product Class 6 : 1,2,4-Oxadiazoles. In: Storr, R. C.; Gilchrist TL, editor. Category 2, Hetarenes and Related Ring Systems, Five-Membered Hetarenes with Three or More Heteroatoms. 2004. p. 127–84.

44. Filho RAWN, Bezerra NMM, Guedes JM, Srivastava RM. An Easy Synthesis of 3,5-Disubstituted 1,2,4-Oxadiazoles from Carboxylic Acids and Arylamidoximes Mediated by Ethyl Chloroformate. J Braz Chem Soc. 2009;20(7):1365–9.

45. Liang G, Feng DD. An Improved Oxadiazole Synthesis Using Peptide Coupling Reagents. Tetrahedron Lett. 1996;37:6627–30.

46. Deegan TL, Nitz TJ, Cebzanov D, Pufko DE, Porco JA. Parallel Synthesis of 1,2,4-Oxadiazoles using CDI activation. Bioorg Med Chem Lett. 1999;9:209–12.

47. Yarovenko VN, Taralashvili VK, Zavarzin I V., Krayushkin MM. New synthesis of 1,2,4-

oxadiazoles. Tetrahedron. 1990;46(11):3941–52.

48. Diana GD, Volkots DL, Nitz TJ, Bailey TR, Long MA, Vescio N, et al. Oxadiazoles as Ester Bioisosteric Replacements in Compounds Related to Disoxaril. Antirhinovirus Activity. J Med Chem. 1994;37:2421–36.

49. Bures F. Fundamental aspects of property tuning in push–pull molecules. RSC Adv. 2014;4:58826–51.

50. Wong MY, Leung LM. Phenothiazine-oxadiazole push-pull fl uorophores : Combining high quantum ef fi ciency , excellent electrochemical stability and facile functionalization. Dye Pigment [Internet]. 2017;145:542–9. Available from: http://dx.doi.org/10.1016/j.dyepig.2017.06.054

51. Zhu L, Gu C, He Y, Wang G. Study on a highly selective fluorescent chemosensor for Cu2+ and its direct sensing for proton based on 1,3,4-oxadiazole. J Lumin. 2014;153:439–45.

52. Zhou J, Tang X, Cheng J, Ju Z, Yang L, Liu W, et al. An 1,3,4-oxadiazole-based OFF–ON fluorescent chemosensor for Zn2+ in aqueous solution and imaging application in living cells. Dalt Trans. 2012;41(35):10626–32.

53. Landis CA, Dhar BM, Lee T, Sarjeant A, Katz HE. Syntheses, Solid State Structures, and Electrical Properties of Oxadiazole-Based Oligomers with Perfluorinated Endgroups. J Phys Chem C. 2008;112:7939–45.

54. Wang C, Jung G, Batsanov AS, Bryce R, Petty MC. New electron-transporting materials for light emitting diodes: 1,3,4-oxadiazole–pyridine and 1,3,4-oxadiazole–pyrimidine hybrids. J Mater Chem. 2002;12:173–80.

55. Liu R, Xu X, Peng J, Yao C, Wang J, Li L. Solution-processed oxadiazole-based electron-transporting layer for white organic light-emitting diodes. RSC Adv [Internet]. 2015;5:36568–74. Available from: http://dx.doi.org/10.1039/C5RA04599A

56. Lee J, Shizu K, Tanaka H, Nomura H, Yasuda T, Adachi C. Oxadiazole- and triazole-based highly-efficient thermally activated delayed fluorescence emitters for organic light-emitting diodes. J Mater Chem C. 2013;1(30):4599.

57. Kulkarni AP, Tonzola CJ, Babel A, Jenekhe SA. Electron Transport Materials for Organic Light-Emitting Diodes. Chem Mater. 2004;16:4556–73.

58. Bostro J, Hogner A, Llina A, Wellner E, Plowright AT. Oxadiazoles in Medicinal Chemistry. J Med Chem. 2012;55:1817–30.

59. Spink E, Ding D, Peng Z, Boudreau MA, Leemans E, Lastochkin E, et al. Structure − Activity Relationship for the Oxadiazole Class of Antibiotics. J Med Chem. 2015;58(3):1380–9.

60. Gold B, Smith R, Nguyen Q, Roberts J, Ling Y, Quezada LL, et al. Novel Cephalosporins Selectively Active on Nonreplicating Mycobacterium tuberculosis. J Med Chem. 2016;59:3027–44.

61. Rajagopalan S, Raman PVA. A Publication of Reliable Methods for the Preparation of Organic Compounds: 2-Furanacrylic acid. Org Synth. 1945;25:51.

62. Burja B, Kocevar M, Polanc S. A simple approach to pyrazol-3-ones via diazenes. Tetrahedron. 2009;65:8690–6.

63. Sahyoun T, Arrault A, Schneider R. Amidoximes and Oximes: Synthesis, Structure, and Their Key Role as NO Donors. Molecules. 2019;24(13):2470.

64. Jonnatan C, Barros P, Freitas JJRDE, Oliveira RNDE, Filho JRDE. Synthesis of amidoximes using an efficient and rapid ultrasound method. J Chil Chem Soc. 2011;56:721–2.

65. Pitasse-santos P, Sueth-santiago V, Lima MEF. 1,2,4- and 1,3,4-Oxadiazoles as Scaffolds in the Development of Antiparasitic Agents. J Braz Chem Soc. 2018;29(3):435–56.

66. Lakowicz JR (Ed. . Principles of Fluorescence Spectroscopy. In: Instrumentation for Fluorescence Spectroscopy. Springer, Boston, MA; 2006. p. 1–26.

67. Grabolle M, Spieles M, Lesnyak V, Gaponik N, Eychmuller, Alexander *,‡ Resch-Genger U. Determination of the Fluorescence Quantum Yield of Quantum Dots : Suitable Procedures and Achievable Uncertainties. Anal Chem. 2009;81(15):6285–94.

68. Brouwer AM. Standards for photoluminescence quantum yield measurements in solution (IUPAC Technical Report)*. Pure Appl Chem. 2011;83(12):2213–28.

69. Imato K, Enoki T, Uenaka K, Ooyama Y. Synthesis, photophysical and electrochemical properties of pyridine, pyrazine and triazine-based (D–π–)2A fluorescent dyes. Beilstein J Org Chem. 2019;15:1712–21.

70. Becke AD. Perspective: Fifty years of density-functional theory in chemical physics. J Chem Phys. 2014;140:18A301-1-18A301-17.

71. G.E.S.M.J. Frisch, G.W. Trucks, H.B. Schlegel, B.M.M.A. Robb, J.R. Cheeseman, G. Scalmani, V. Barone, H.P.H.G.A. Petersson, H. Nakatsuji, M. Caricato, X. Li, M.H.A.F. Izmaylov, J. Bloino, G. Zheng, J.L. Sonnenberg, T.N.M. Ehara, K. Toyota, R. Fukuda, J. H DJF. Gaussian 09. 2009.

72. Becke AD. Density-functional thermochemistry. III. The role of exact exchange. J Chem Phys. 1993;98(7):5648–52.

73. Lee C, Yang W, Parr RG. Development of the Colic-Salvetti correlation-energy formula into a functional of the electron density. Phys Rev B. 1988;37(2):785–9.

74. Olutas M, Sagırlı A. Solvatochromic and solid-state emissive azlactone-based AIEE-active organic dye: Synthesis, photophysical properties and color-conversion LED application. J Mol Liq. 2020;313:113482.

75. Bernard Valeur MNB-S. Molecular Fluorescence: Principles and Applications. John Wiley & Sons; 2013. 592 p.

76. Hrdlovic P, Donovalova J, Stankovicova H, Gaplovsky A. Influence of Polarity of Solvents on the Spectral Properties of Bichromophoric Coumarins. Molecules. 2010;15:8915–32.

77. Souza DR da S, Caminhas LD, Mesquita JP de, Pereira FV. Luminescent carbon dots obtained from cellulose. Mater Chem Phys. 2018;203:148–55.

78. Sahu S, Behera B, Maiti TK, Mohapatra S. Simple one-step synthesis of highly luminescent carbon dots from orange juice: Application as excellent bio-imaging agents. Chem Commun. 2012;48(70):8835–7.

79. Jhonsi MA, Thulasi S. A novel fluorescent carbon dots derived from tamarind. Chem Phys Lett [Internet]. 2016;661:179–84. Available from: http://dx.doi.org/10.1016/j.cplett.2016.08.081

7. APPENDICES

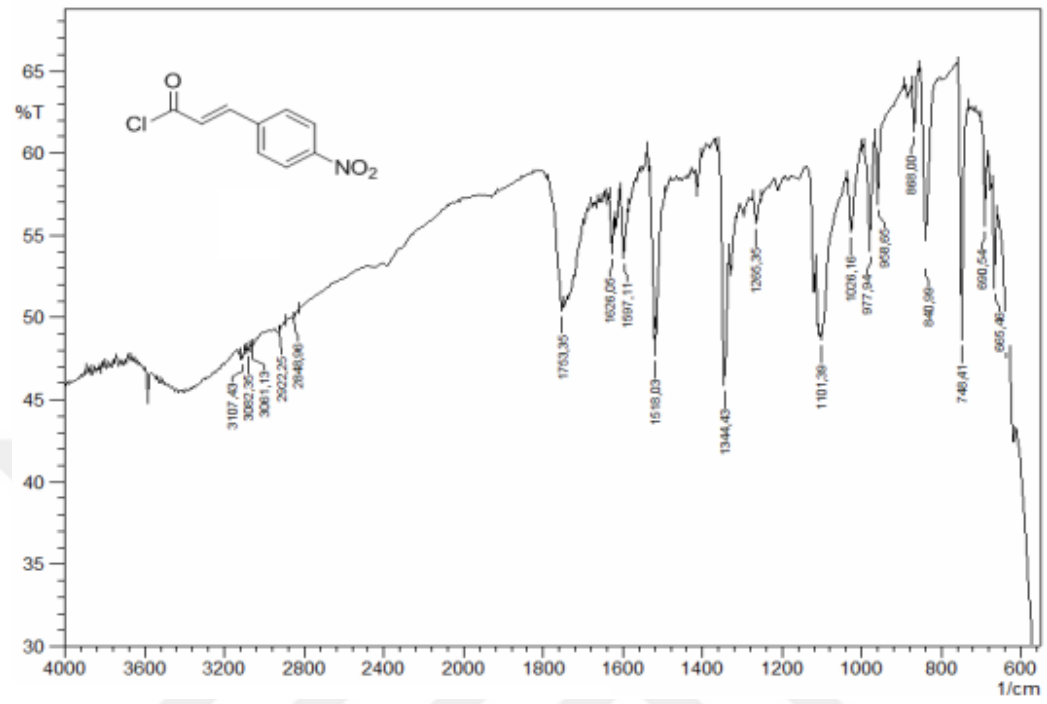

Figure 7.1. IR spectrum of p-nitrocinnamoyl chloride **21c**.

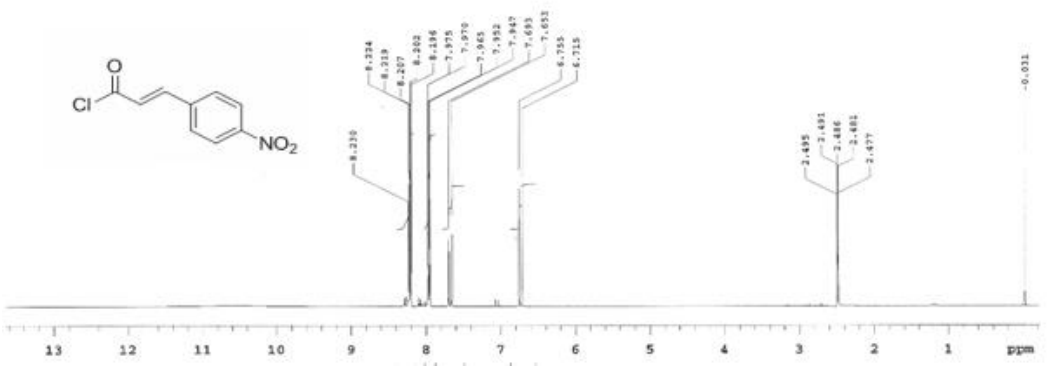

Figure 7.2. [1]H NMR spectrum of p-nitrocinnamoyl chloride **21c**.

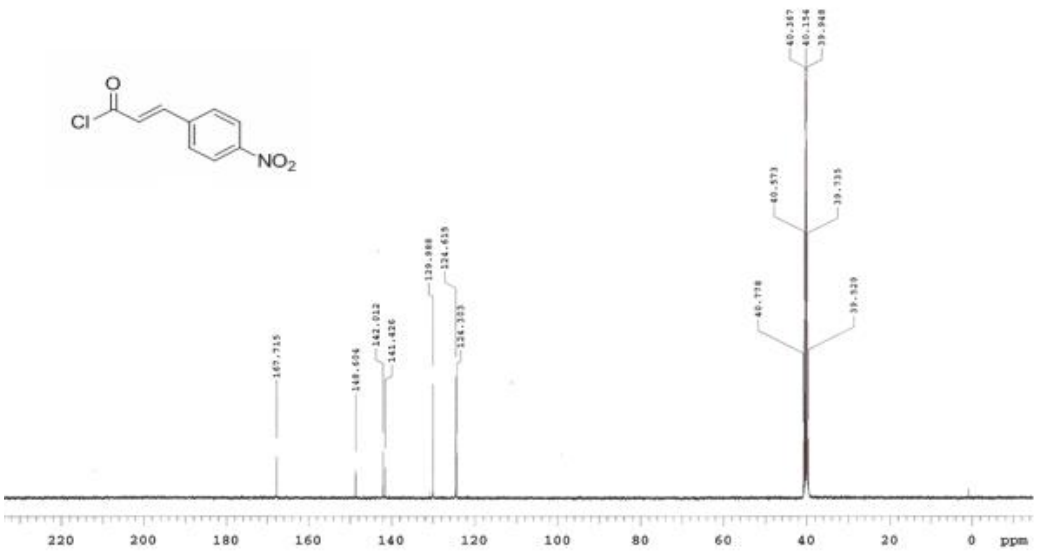

Figure 7.3. ^{13}C NMR spectrum of p-nitrocinnamoyl chloride **21c**.

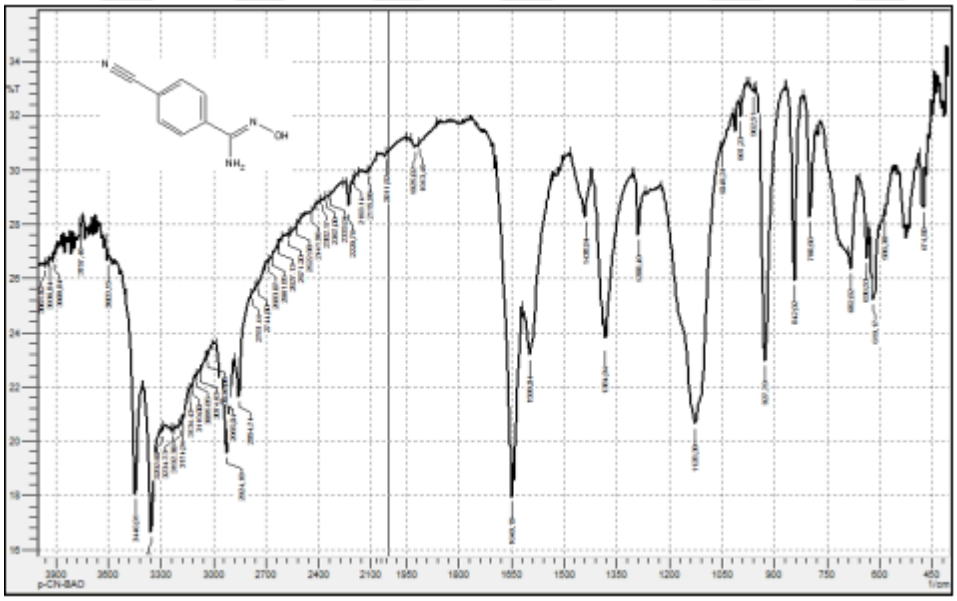

Figure 7.4. IR spectrum of p-cyanobenzamidoxime **9a**.

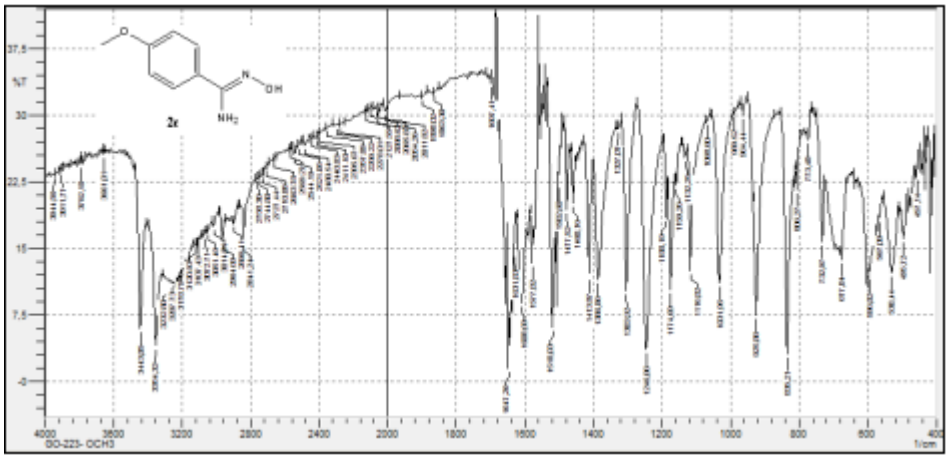

Figure 7.5. IR spectrum of *p*-methoxybenzamidoxime **9b**.

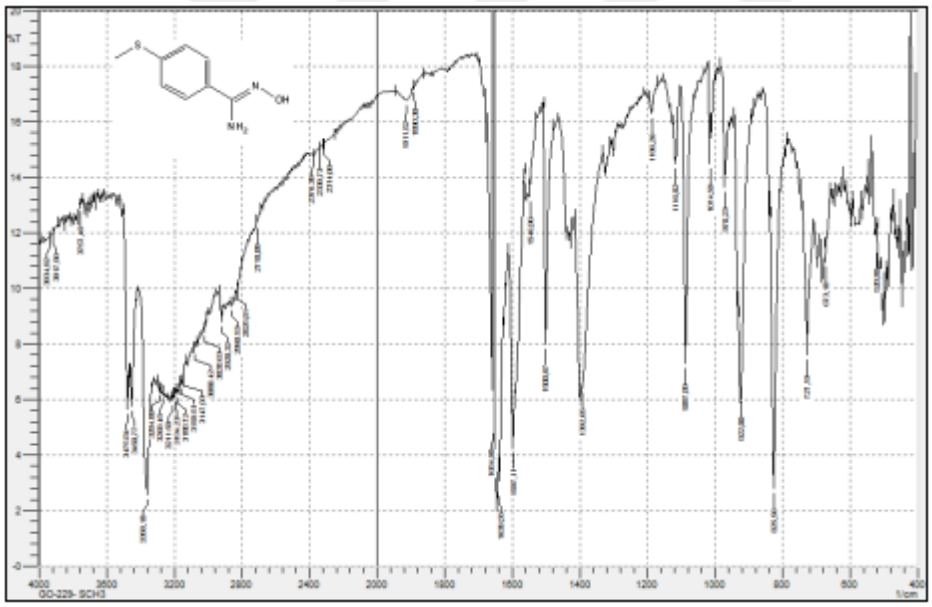

Figure 7.6. IR spectrum of *p*-methylthiobenzamidoxime **9c**.

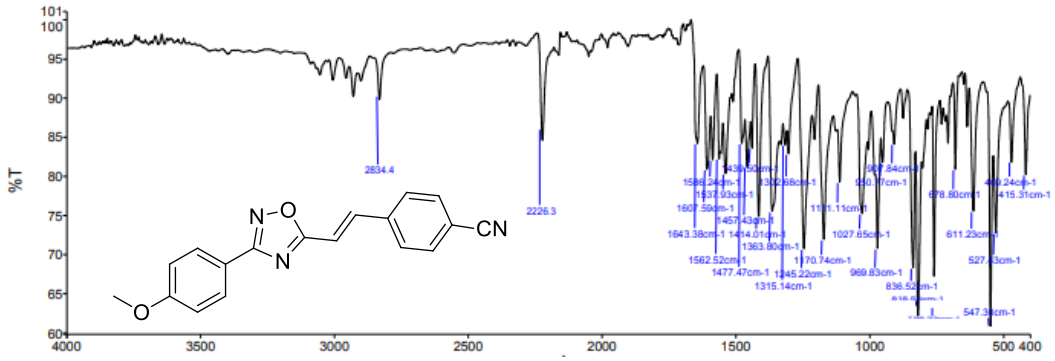

Figure 7.7 IR spectrum of compound **23a** (RXN-1).

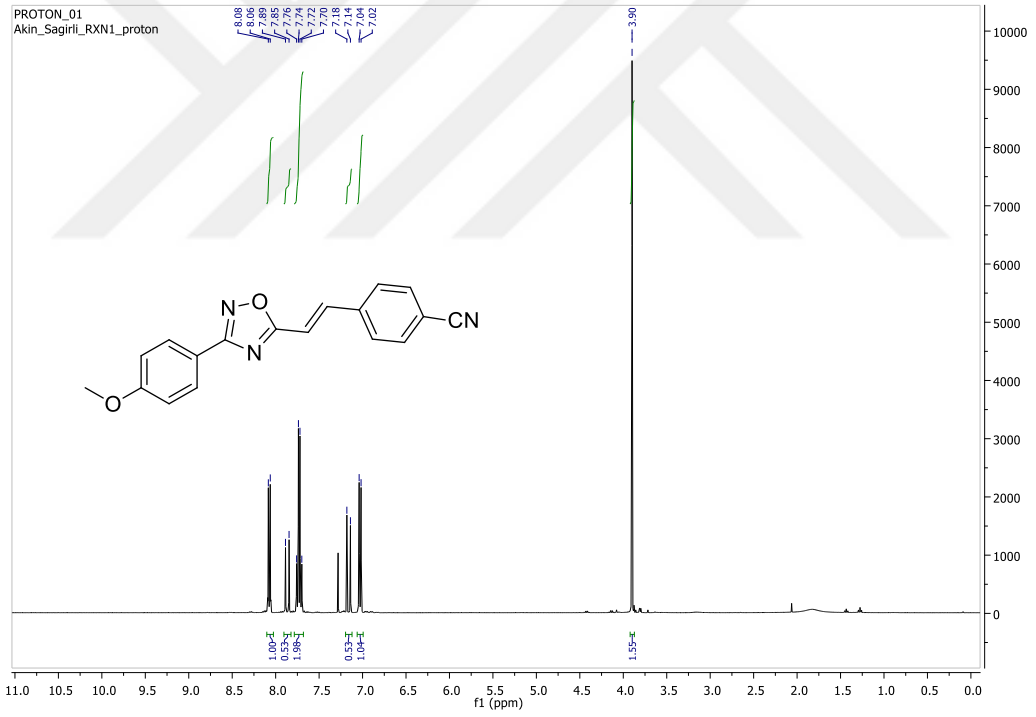

Figure 7.8 ^{1}H NMR spectrum of compound **23a** (RXN-1).

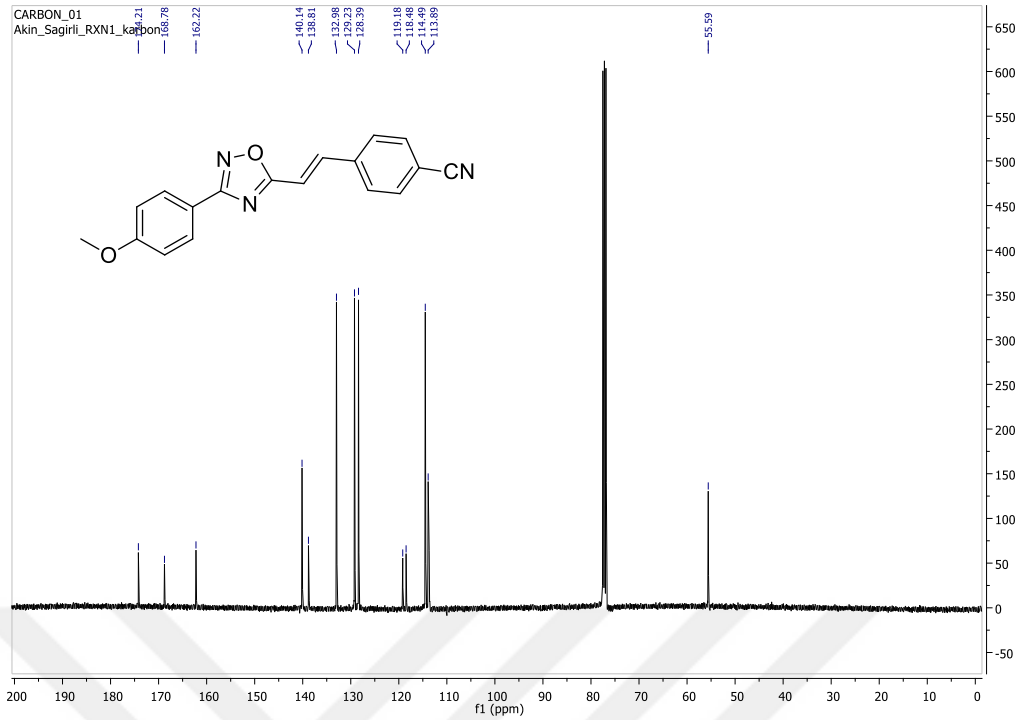

Figure 7.9. ^{13}C NMR spectrum of compound **23a** (RXN-1).

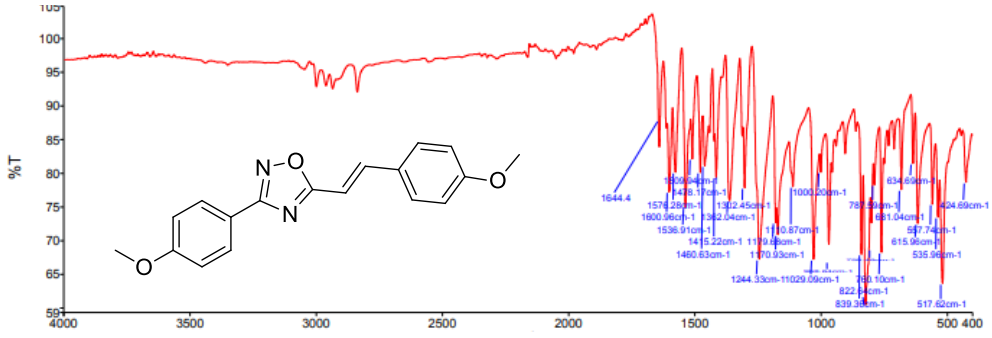

Figure 7.10. IR spectrum of compound **23b**

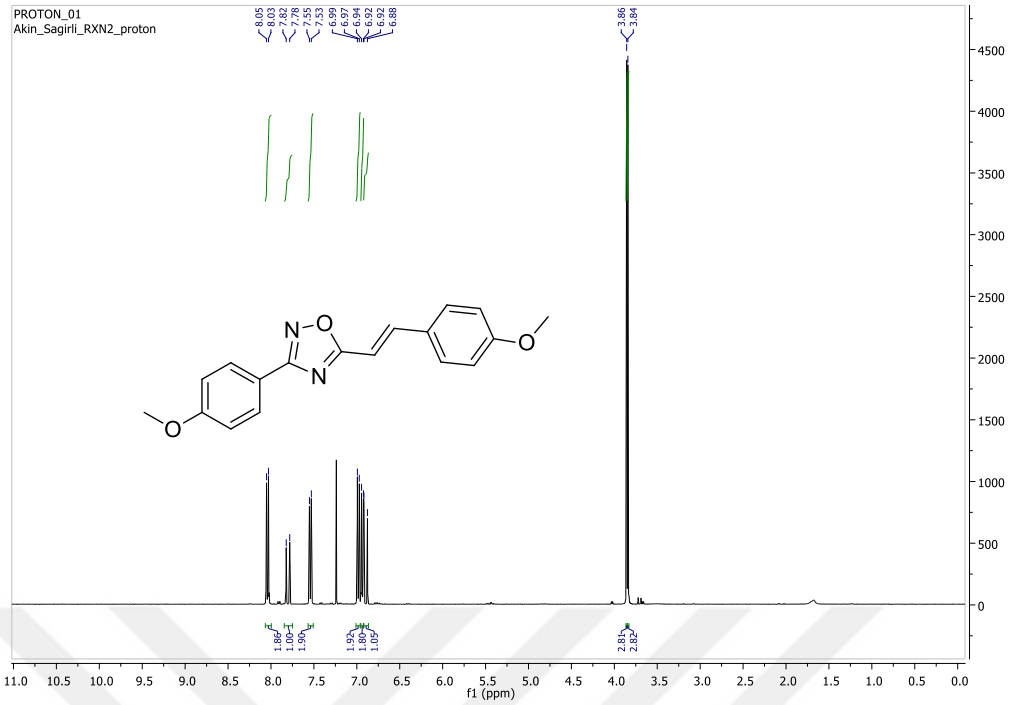

Figure 7.11. ^{1}H NMR spectrum of compound **23b** (RXN-2).

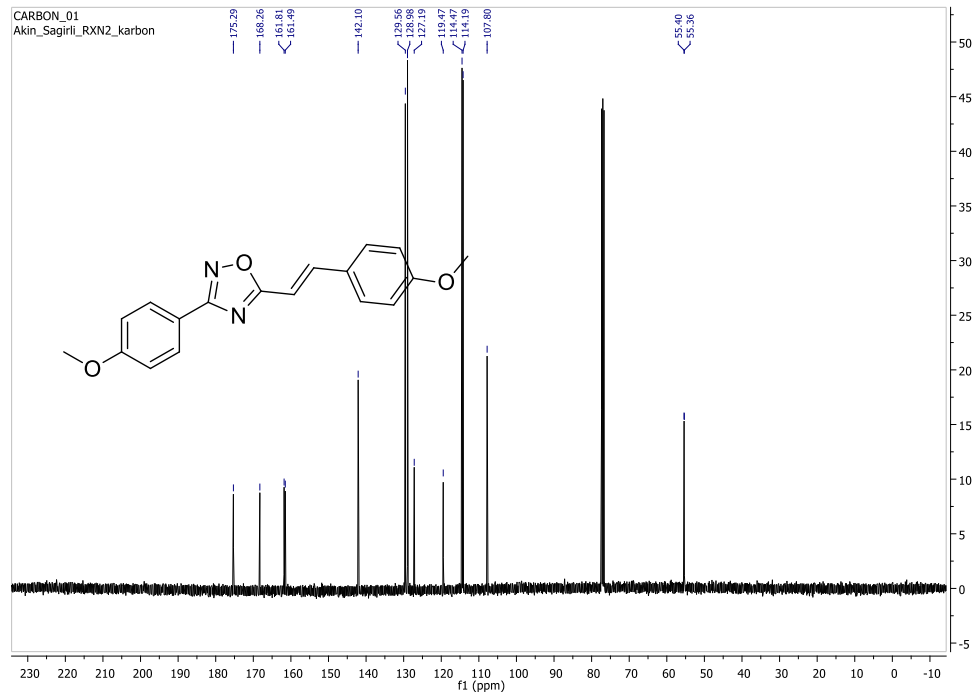

Figure 7.12. ^{13}C NMR spectrum of compound **23b** (RXN-2).

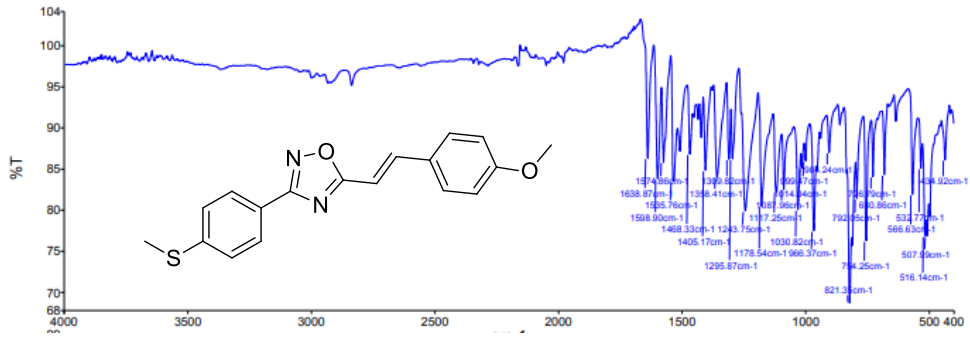

Figure 7.13. IR spectrum of compound **23c** (RXN-3).

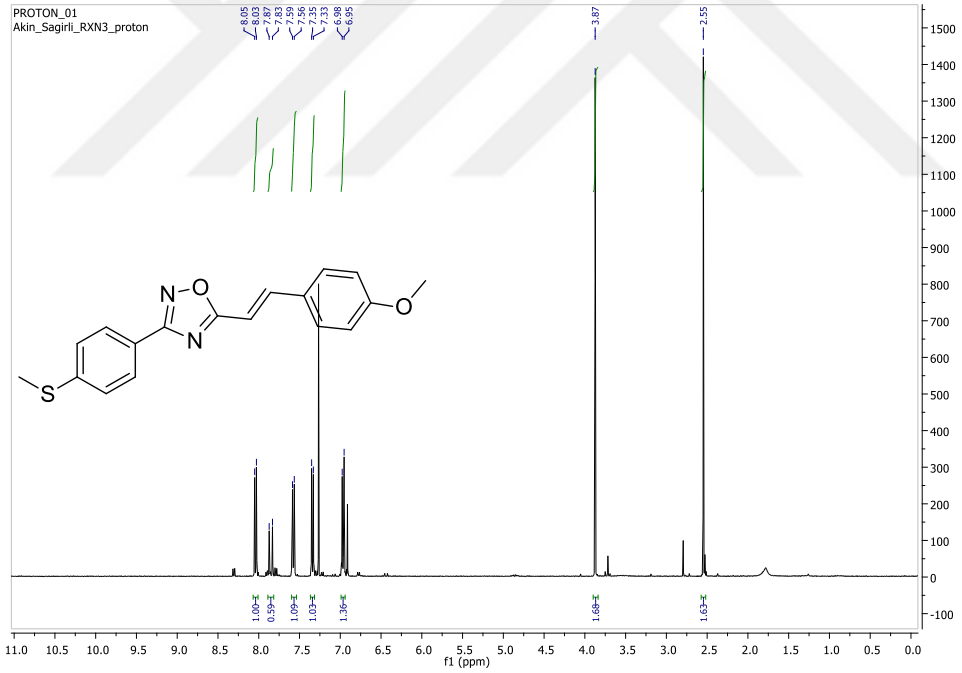

Figure 7.14 ^{1}H NMR spectrum of compound **23c** (RXN-3).

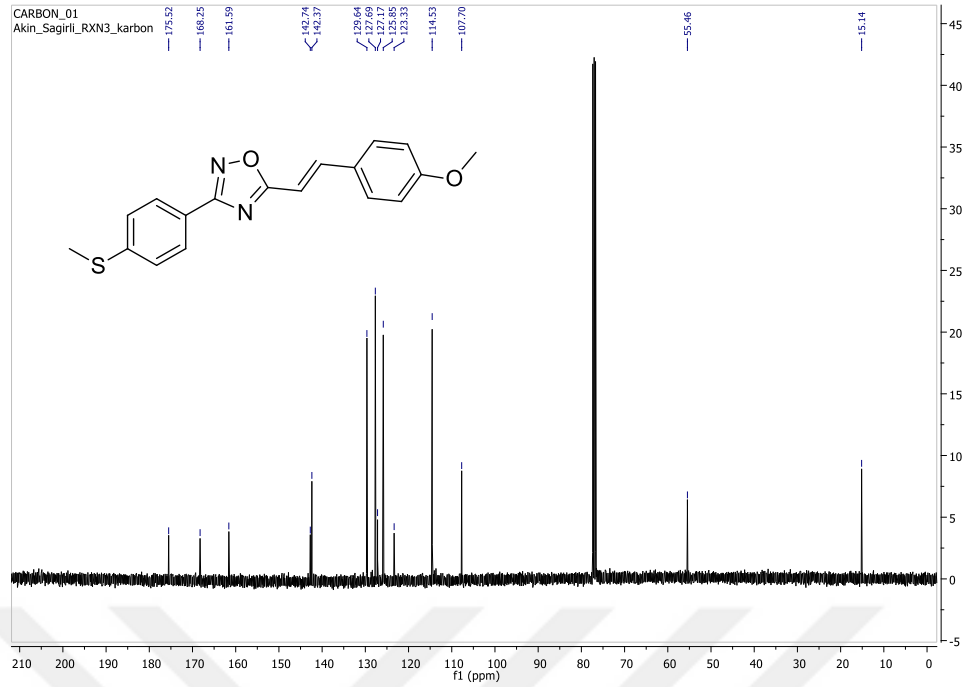

Figure 7.15. ^{13}C NMR spectrum of compound **23c** (RXN-3).

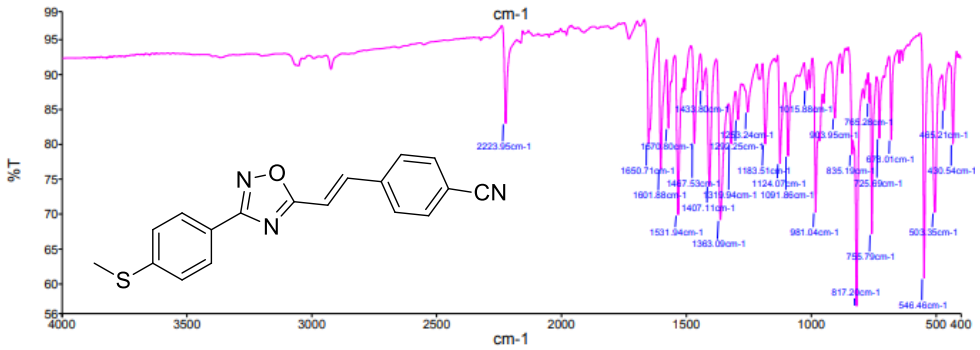

Figure 7.16. IR spectrum of compound **23d** (RXN-4).

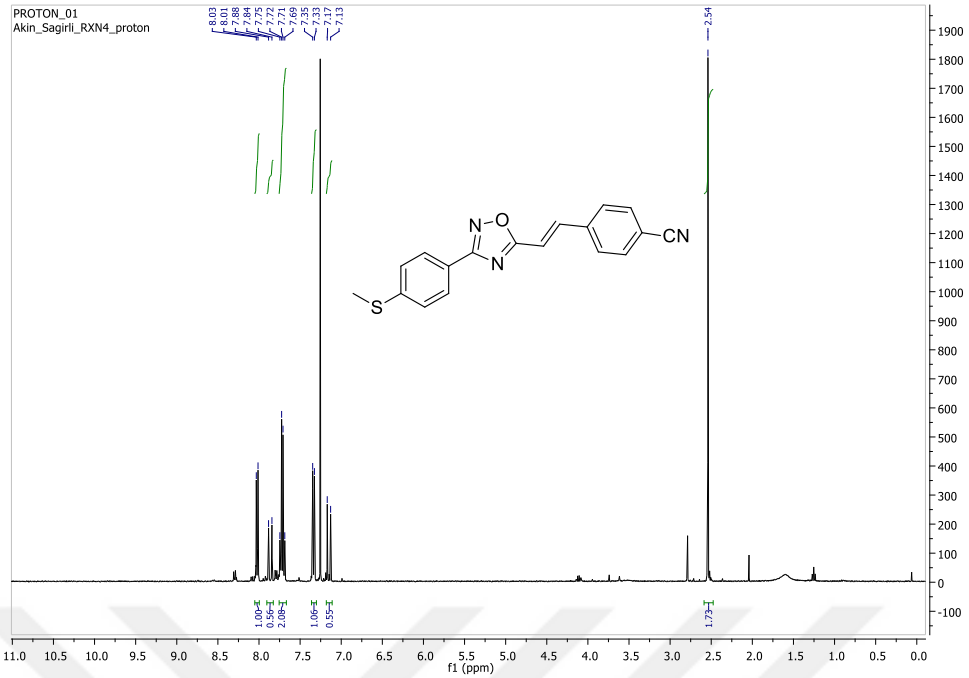

Figure 7.17. [1]H NMR spectrum of compound **23d** (RXN-4).

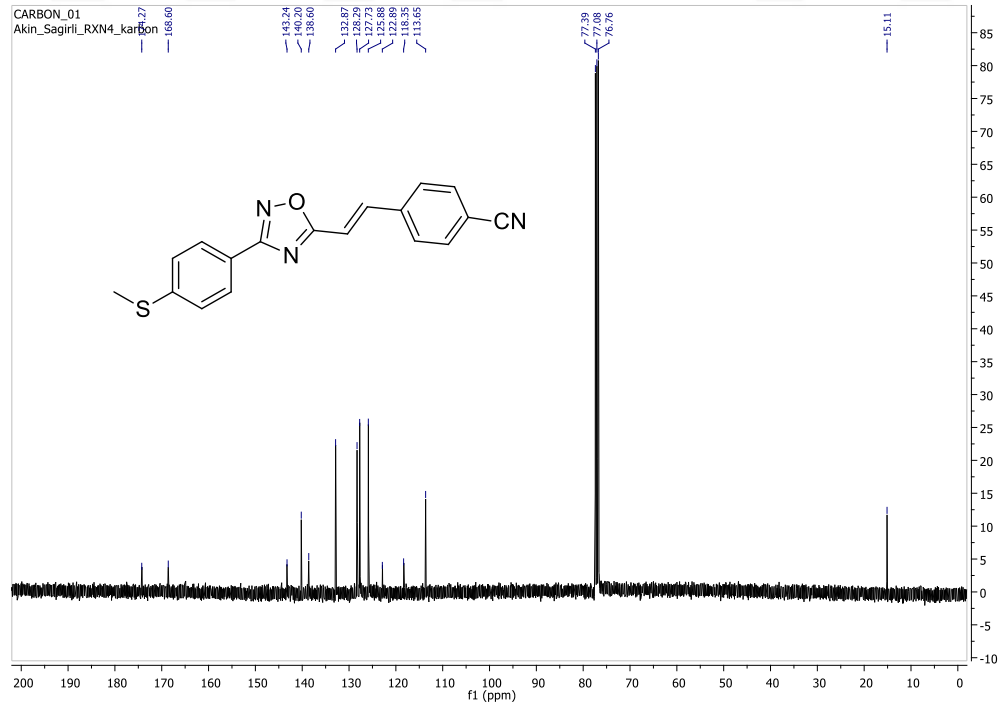

Figure 7.18. [13]C NMR spectrum of compound **23d** (RXN-4).

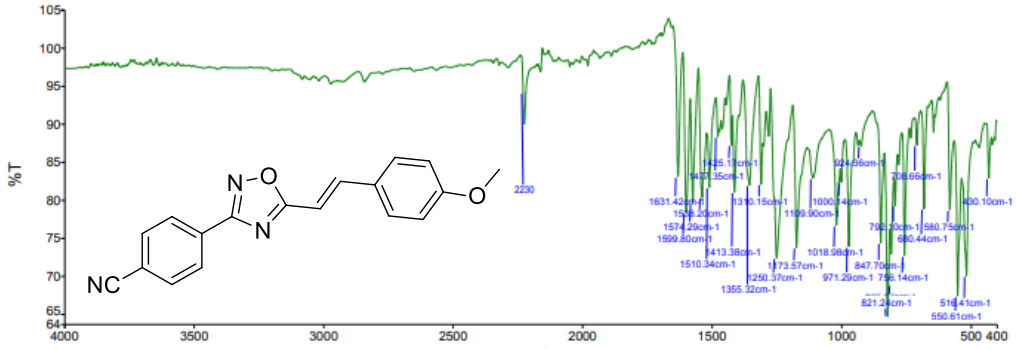

Figure 7.19 IR spectrum of compound **23e** (RXN-5).

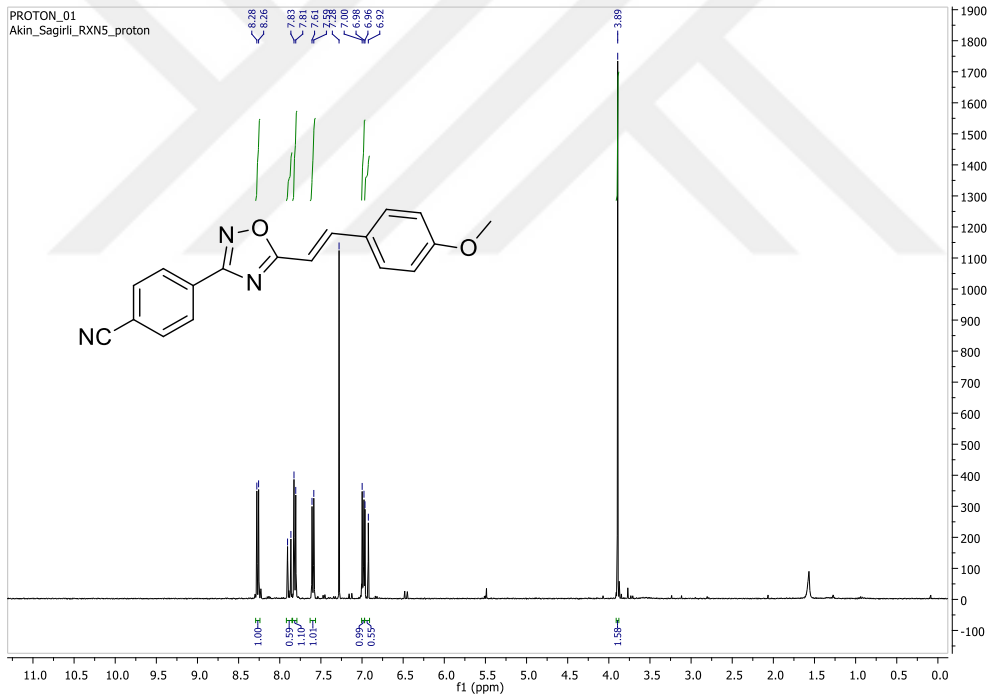

Figure 7.20. ^{1}H NMR spectrum of compound **23e** (RXN-5).

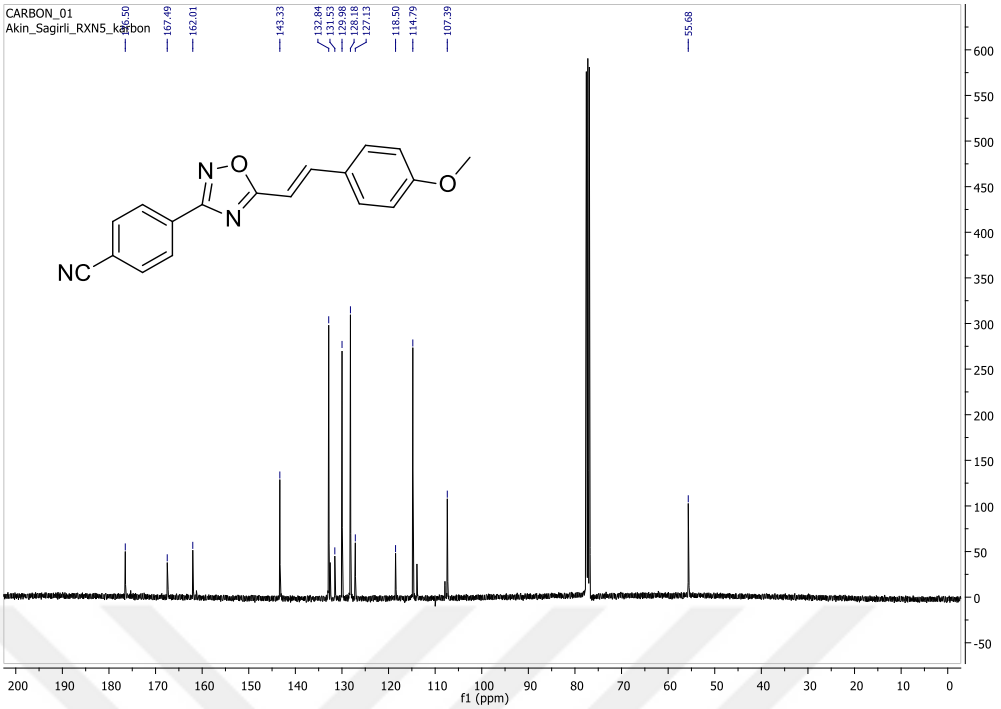

Figure 7.21 ^{13}C NMR spectrum of compound **23e** (RXN-5).

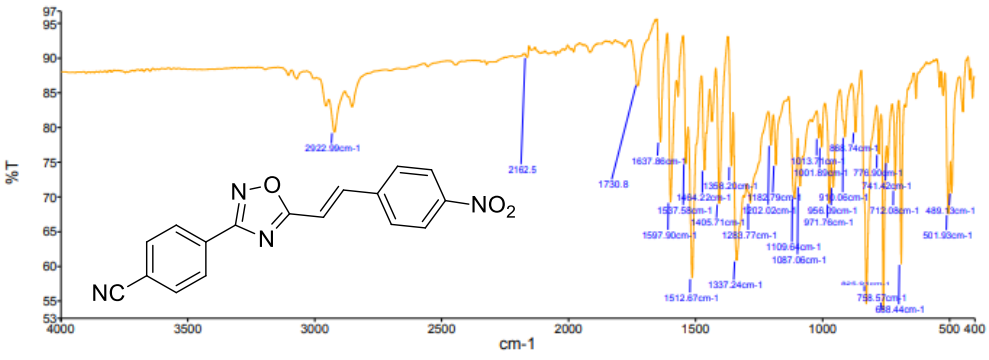

Figure 7.22. IR spectrum of compound **23f** (RXN-6).

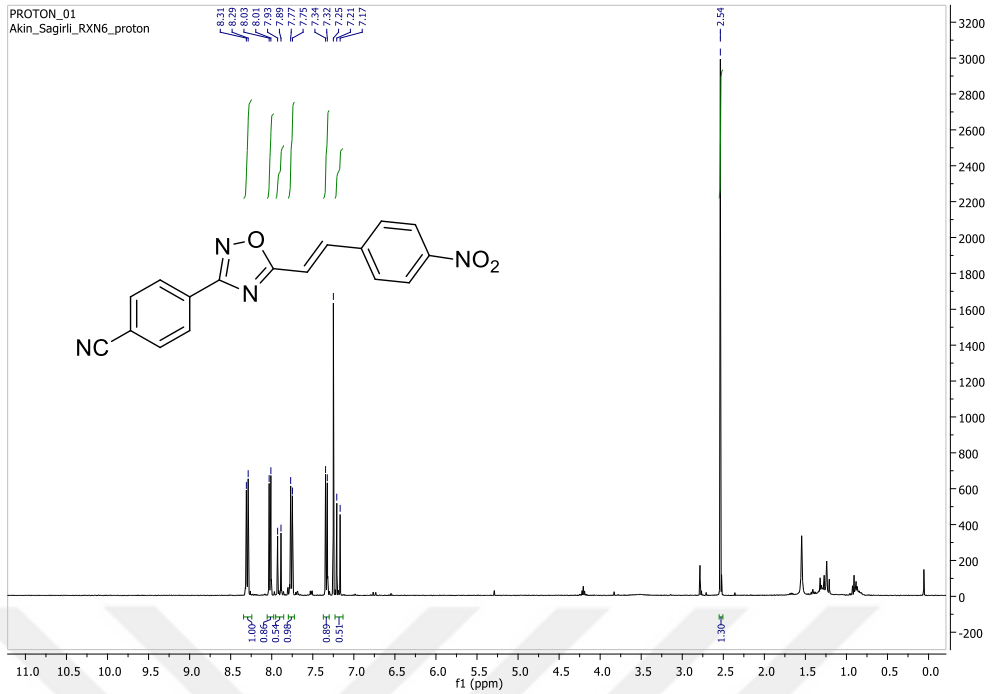

Figure 7.23 ^{1}H NMR spectrum of compound **23f** (RXN-6).

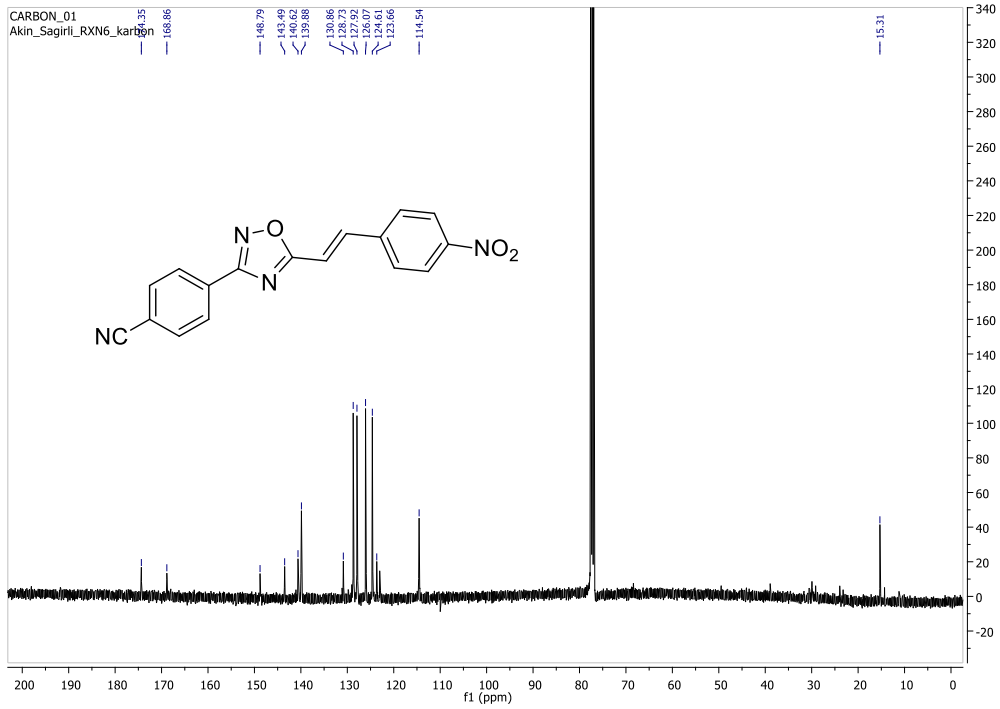

Figure 7.24 ^{13}C NMR spectrum of compound **23f** (RXN-6).